Master's Thesis

In vitro glycoengineering of a monoclonal antibody produced in insect cells

Anastasiia Zhurina

University of Jyväskylä

Department of Biological and Environmental Science

27 May 2024

UNIVERSITY OF JYVÄSKYLÄ, Faculty of Mathematics and Science
Department of Biological and Environmental Science
Master's Degree Programme in Nanoscience

Zhurina, Anastasiia

In vitro glycoengineering of a monoclonal antibody produced in insect cells

MSci Thesis
50 p., 1 appendix (2 p.)

Supervisors: Dr. Karim Enrique Jaén Chávez, Dr. Mariana Juárez-Osorio, Prof. Janne Ihalainen

Tarkastajat:

May 2024

Keywords: effector functions, glycoengineering, homogenous glycoprofile, Lepidopteran insect cells, monoclonal antibody

Sugar modifications, in particular, *N*-glycans, largely determine protein quality, functionality, and, in case of therapeutic biomolecules, safety. Therapeutic monoclonal antibodies (mAbs) generate immune response through effector functions, for which they require complex *N*-glycans with high levels of galactose, sialic acids, and lack of core fucose, often unachievable in commercial production yielding suboptimal and heterogenous glycosylation pattern. Current glycoengineering strategies successfully tailor *N*-glycan composition on mAbs, yet fail to improve glycoprofile homogeneity. In this work, a recently developed cell-free *in vitro* glycoengineering approach was evaluated for generation of homogenous fully galactosylated *N*-glycoforms on therapeutic effector antibody Rituximab, characterized by low levels of galactose and glycan homogeneity in the originally marketed product. With an aim of targeting commercial mAbs, an industry-oriented protein production and glycoengineering strategy was designed on the basis of Lepidopteran insect cells. Rituximab was expressed in baculovirus-infected HighFive™ cells to obtain highly uniform starting *N*-glycoprofile, which was sequentially modified by recombinant human β-1,2 N-acetylglucosamintransferases I and II (MGAT1ΔTM and MGAT2ΔTM), and β-1,4-galactosyltransferase (GalTΔTM). The enzymatic cascade remodelled simple insect cell oligosaccharides on protein A-immobilized mAb species into complex human-like structures with a near 100% conversion rate. Recombinant enzyme production was tested in HighFive™ host, for which a functional expression protocol was developed, and a promising purification approach incorporating solubilizers was proposed. Production of Rituximab in HighFive™ cells was challenged by poor mAb assembly despite optimization of cell culture conditions. The results indicated a need for significant effort in improving insect cell-based protein production strategy to achieve higher enzyme and antibody yields. With suggested directions for further research, assessed *in vitro* glycoengineering platform can become an effective toolbox for generating high-efficacy therapeutic mAbs in industrial settings.

TABLE OF CONTENTS

TERMS AND ABBREVIATIONS

Terms

HighFive™	Commercial name for *Trichoplusia ni* BTI-Tn-5B1-4
***N*-glycan fingerprint**	Electropherogram aligned on migration time axis (x-) and normalized on fluorescence signal intensity axis (y-)

Abbreviations

AcMNPV	*Autographa californica* multiple nucleopolyhedrovirus
CDCCM	Chemically defined complete culture medium
xCGE-LIF	Capillary gel electrophoresis with laser-induced fluorescence detection
DO	Dissolved oxygen
dV	Dual expression transfer vector
E.coli	*Escherichia coli*
Gal	Galactose
(β4)GalT(1)	β-N-acetylglucosaminylglycopeptide β-1,4-galactosyltransferase 1
GlcNAc	N-acetylglucosamine
HC	Heavy chain of an antibody
IgG	Immunoglobulin G
IP	Infectious particles
IVGE	*In vitro* glycoengineering
LC	Light chain of an antibody
mAb	Monoclonal antibody
Man	Mannose
MGAT1	α-1,3-Mannosyl-Glycoprotein 2-β-N-Acetylglucosaminyltransferase
MGAT2	α-1,6-Mannosyl-Glycoprotein 2-β-N-Acetylglucosaminyltransferase
MOI	Multiplicity of infection
MTU	Migration time units after alignment to internal standards
mV	Monopromoter transfer vector
PTM	Post-translational modification
rBV	Recombinant baculovirus
SDS-PAGE	Sodium dodecyl-sulphate polyacrylamide gel electrophoresis
Sf9	*Spodoptera frugiperda* clonal isolate 9
ΔTM	Without transmembrane domain
TPH	Total peak height
UDP	Uridine diphosphate
VCC	Viable cell concentration

1 INTRODUCTION

Glycosylation is among the most common and structurally diverse post-translational modifications found on proteins in all domains of life. Comprised of monosaccharides covalently bound through glycosidic linkages, glycan structures are attached to particular amino acid residues, and play a major role in the functionality and quality of a protein molecule (Gagneux et al. 2022). Through multiple non-covalent interactions with the glycoprotein, carbohydrates increase solubility, folding efficiency, thermal and conformational stability of the biomolecule, prevent proteolytic and chemical degradation (Ma et al. 2020). Individual monosaccharides of a glycan also participate in molecular and cellular interactions, signalling pathways, and binding mechanisms (Jaroentomeechai et al. 2022). Thus, biological activity and quality of a glycoprotein are heavily mediated by the glycoforms it bears and their structure (Gagneux et al. 2022). Two major glycosylation groups are outlined based on glycoprotein attachment site: *N*-glycans and *O*-glycans. *N*-glycans are linked to the nitrogen atom of the amide group in Asparagine residues; these glycoforms are particularly abundant in eukaryotic secretory and cell surface proteins (Varki et al. 2015). All *N*-glycans possess a core structure of Man3 (Stanley et al. 2009), trimannosyl-chitobiose core with two N-acetylglucosamine (GlcNAc) moieties connected via β1,4-glycosidic bond, and three Mannose (Man) residues in different positions and linkages (Figure 1A). Further structural variations are species-dependent. Despite the overwhelming diversity, *N*-glycans are classified into 3 main types: high-mannose, complex, and hybrid (Figure 1). Complex glycans, mostly found in mammalian organisms, possess the highest monosaccharide variability, which modulates a large number of protein characteristics (Varki et al. 2015). Due to the unprecedented role in determining quality, functionality, and biological activity of proteins, *N*-glycoprofile requires stringent control on those proteins where these aspects are crucial (Ma et al. 2020). Therapeutic proteins represent the major share of such biomolecules, where *N*-glycan composition is a critical attribute. Together with defining therapeutic effect of a glycoprotein, monosaccharides of a carbohydrate also affect immunogenicity of the therapeutic protein, thus becoming a parameter of active monitoring and optimization (Ma et al. 2020).

The largest share of therapeutic proteins for human use is occupied by monoclonal antibodies, represented mainly by immunoglobulins G (IgGs), ~150 kDa heterodimers comprised of two light chains (each 25 kDa) and two heavy chains (around 50 kDa), intra- and interlinked through disulphide bonds (Figure 2A) (Dimitrov 2012). Highly variable regions in the N-termini of heavy and light chains constitute fragment antigen binding (F_{ab}) domain, responsible for highly selective binding of antigens and their subsequent neutralization. Conserved domains of heavy chains in the C-terminus of an IgG form crystallisable fragment (F_c), where each heavy chain bears a single *N*-glycosylation site in Asparagine

residue 297 (Asn297) (Figure 2B) (Higel et al. 2016). *In vivo*, endogenous IgGs are synthesized by B-cells in response to a pathogen, with the purpose of F_{ab} domain-induced binding and neutralization of the antigens – this immune function comprises the basis of the therapeutic effect of an IgG molecule (Alberts et al. 2002). Among 4 subclasses of IgGs, IgG_1 and IgG_3 enhance their therapeutic effect through effector functions, a set of mechanisms mediated by the F_c domain. Following F_{ab}-mediated binding of an IgG to the target antigen exhibited on infected or tumour cells, specific sites in the F_c region recognise and bind receptors and immune system proteins (Lu et al. 2018). As a result, cascades of reactions leading to elimination of the marked cell by innate immune system pathways are initiated. Two most abundant effector functions are antibody-dependent cellular cytotoxicity (ADCC), where F_c domain is bound to FcγRIII receptor of natural killer (NK) cells and macrophages, and complement-dependent cytotoxicity (CDC), activated through association of F_c receptor and C1q complement component protein (Figure 3A) (Higel et al. 2016). The magnitude of ADCC and CDC is exclusively dependent on the *N*-glycans of an $IgG_{1/3}$ (Mastrangeli et al. 2019). An "ideal" glycoform composition that yields most intense effector functions activation has been characterised: a complex bi-antennary glycan S2(α2,6)G2 lacks core fucose, monosaccharide that strongly inhibits ADCC, and contains terminal α1,3-linked galactose and α2,6 N-Acetylneuraminic acid, both proven beneficial for CDC, and, according to certain investigators, to ADCC (Figure 3B) (Mastrangeli et al. 2019). This glycan is thus most desired by the manufacturers of therapeutic mAbs.

Achieving S2(α2,6)G2 structure on therapeutic mAbs is complicated. Most commercial IgGs are produced in mammalian cells, largely in Chinese Hamster Ovary (CHO) and murine myeloma NS0 and Sp2/0 cell lines, due to their production efficiency and human-like PTMs (Dumont et al. 2016). However, glycan profile of proteins produced in these cells significantly differs from the target S2(α2,6)G2: resulting glycoforms contain inconsistent levels of individual monosaccharides, non-human sugar residues, and monosaccharides with glycosidic linkages unnatural to humans (Figure 1B) (Mastrangeli et al. 2019). Batch-to-batch variations in monosaccharide composition originate from fluctuations in bioprocess conditions, while potentially immunogenic sugar residues are host organism-specific. These deviations result in microheterogenous glycoprofile of a therapeutic mAb, comprised of a mixture of glycan structures, where only a small fraction of carbohydrate species activates effector functions to a maximum extent (Higel et al. 2016). Therefore, a strong demand for *N*-glycoprofile optimization on therapeutic IgGs exists.

A substantial amount of effort to improve *N*-glycan composition towards the S2(α2,6)G2 target has been implemented through glycoengineering, a group of methods designed to manipulate therapeutic proteins' glycoprofile. In IgG glycoengineering, research work has primarily focused on cell-based approaches, where glycan biosynthesis pathway is optimized through genetic modifications of producent cell lines (Ma et al. 2020). While these efforts have resulted in an improved share of S2(α2,6)G2 glycans on mAbs, and yielded market-released

glycoengineered antibodies (Beck & Reichert 2012; Cameron & McCormack 2014), full control over the glycosylation pattern has not been achievable due to the complexity of *in vivo* pathways and sensitivity of cells to culture condition variations (Mastrangeli et al. 2019). Alternative glycoengineering methods employ modification of glycans by sequentially applying enzymes that selectively trim, elongate, and link carbohydrates. *In vitro* glycoengineering (IVGE) chemoenzymatically remodels *N*-glycan composition on pure glycoproteins in cell-free environment, thus eliminating interferences associated with the cell-based approach (Mota et al. 2022).

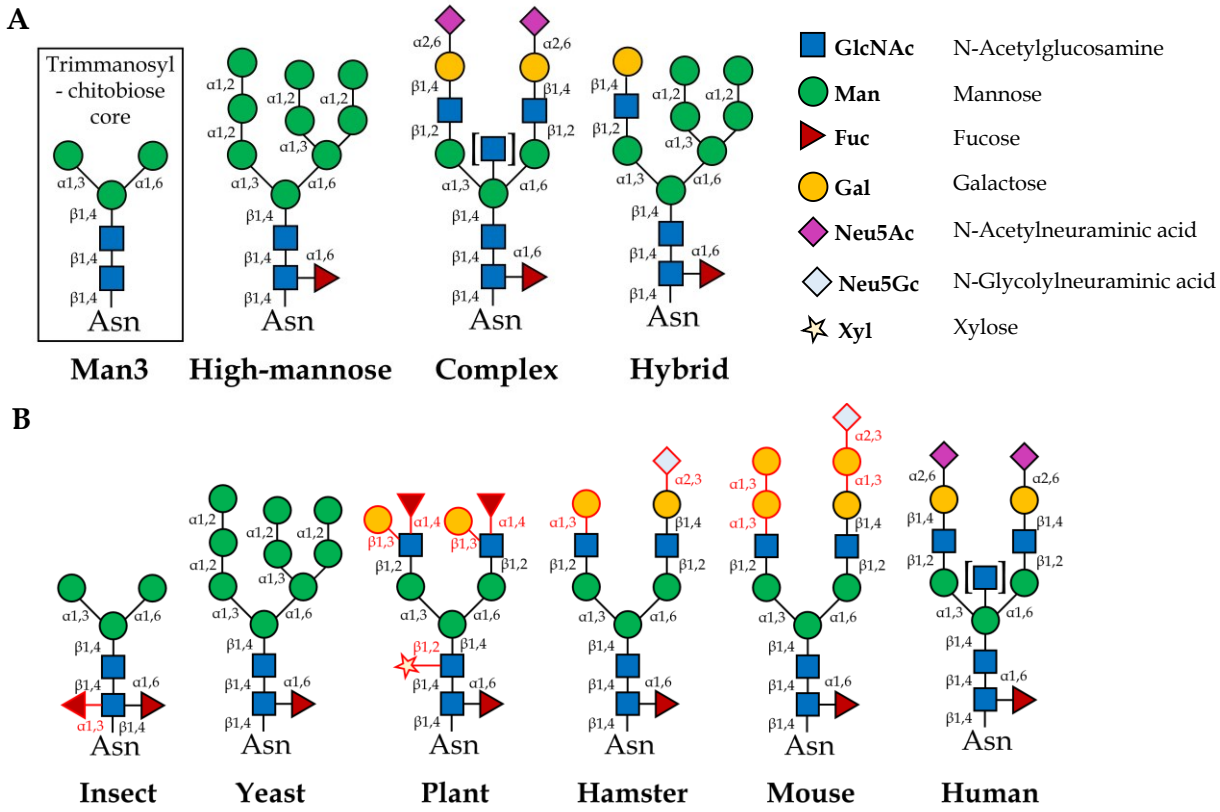

Figure 1. Typical *N*-glycan structures and their diversity in various eukaryotic species. **A)** Three main types of *N*-glycans are high-mannose, complex, and combination of both – hybrid; each *N*-glycan within or outside of this classification bears core structure Man3. **B)** Most commonly investigated eukaryotic hosts for therapeutic protein production vary significantly in *N*-glycan composition: some bear non-human monosaccharides, like Neu5Gc and Xyl (highlighted in red), or those with unnatural to humans linkages like α1,3-Gal and α2,3-Neu5Gc (highlighted in red). Here and further *N*-glycan nomenclature from Varki et al. 2015 is used; depiction of *N*-glycan structures corresponds to the Symbol Nomenclature for Glycans guidelines (Neelamegham et al. 2019).

IVGE has amplified therapeutic efficacy of mAbs, and produced several commercial products with core afucosylation, terminal galactosylation and sialylation (Mastrangeli et al. 2019). Most renown IVGE approach is two-step, starting with complete removal of *N*-glycan from the protein by endoglycosidase

or glycosaminidase digestion, and subsequent reattachment of a pre-assembled correct *N*-glycoform using glycosynthases (Mimura et al. 2018). This strategy has been successfully employed on IgGs produced in several hosts, rendering its wide-range applicability, and has progressed into industrial-scale trials (Mastrangeli et al. 2019). Lesser known and reported IVGE investigations focus on terminal modification of complex IgG *N*-glycans, thus modifying galactosylation and sialylation (Chung et al. 2006; Raju et al., 2001) through use of monosaccharide-specific enzymes – glycosidases, carbohydrate-trimming enzymes, and glycosyltransferases, enzymes selectively elongating glycan structure. None of such, despite successful, strategies, has progressed towards large-scale validation and application, according to available knowledge.

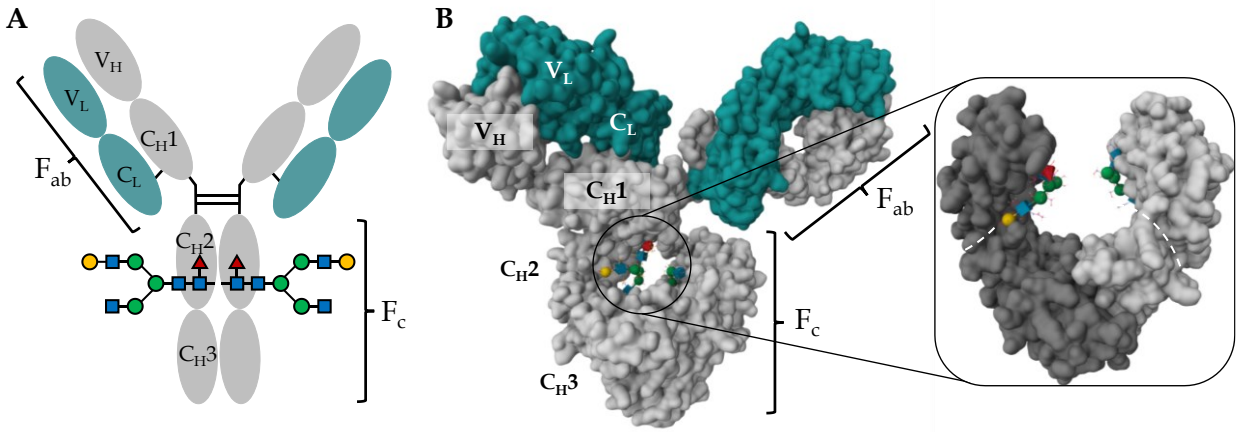

Figure 2. Structure and *N*-glycosylation of a typical IgG; **A)** Schematic representation of IgG: a 150 kDa heterodimer comprised of two heavy chains (in grey) and two light chains (in cyan), linked together by disulphide bonds. Variable C_H1 and V_H subdomains of heavy chain and C_L and V_L of light chain comprise antigen-binding domain F_{ab}. Conserved C_H2 and C_H3 subdomains of heavy chain form crystallizable fragment F_c, where *N*-glycosylation site is found (Asparagine 297); **B)** 3D visualization of IgG structure: Asn297 glycans (here, G1F structures) are inverted into the cavity of F_c domain. In highlighted F_c fragment, C_H2 and C_H3 domains are approximately separated by white dashed lines. Dark grey coloration distinguishes one of two linked heavy chains. 3D figure of the entire IgG is obtained from 1IGY structure from PDB with represented Gaussian surface, F_c fragment in is taken from 5JII with identical representation.

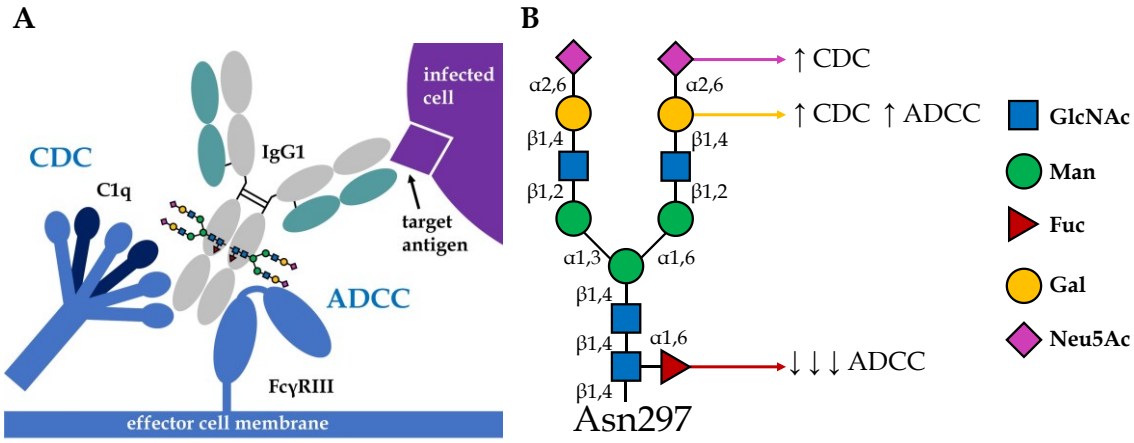

Figure 3. Role of *N*-glycans and specific monosaccharides in effector functions of an $IgG_{1/3}$; **A)** After F_{ab}-mediated binding of a specific antigen (in purple) on an infected/tumour cell (in purple), F_c domain of an effector IgG (heavy chain in grey, light chain in cyan) is able to recruit C1q complement component protein to initiate CDC, as well as induce ADCC through association with FcγRIII receptor found on membranes of NK and macrophage cells; **B)** In these F_c-mediated interactions, Asn297 site *N*-glycans that contain terminal β1,4 galactose (Gal) and α2,6 N-acetylneuraminic acid (Neu5Ac) increase the magnitude of both CDC and ADCC, while core fucose greatly inhibits ADCC. GlcNAc corresponds to N-acetylglucosamine, Man to Mannose, Fuc to Fucose.

This Master thesis work has investigated a novel approach towards therapeutic mAb IVGE through monosaccharide-specific multi-step glycan elongation. Here, variants of Rituximab, a chimeric mouse-human IgG_1 against B-lymphocyte antigen CD20, were produced under chemically defined conditions in baculovirus-infected Lepidopteran insect cells with the purpose of developing Rituximab *N*-glycans with simple side chains into terminally galactosylated bi-antennary structures. For that, three recombinant Leloir glycosyltransferases were employed (Figure 4). Among all *N*-glycan producing organisms, cells of Lepidoptera insect order generate relatively homogenous paucimannose *N*-glycans, closest in structure to the Man3 core (Figure 1) (Palomares et al. 2021), thus serving a near-perfect substrate for various glycan remodelling. Cell-free glycan modification was performed via *in vitro* cell-free enzymatic reaction cascade on protein A-immobilized antibody. First, we applied recombinant α-1,3-mannosyl-glycoprotein 2-β-N-acetylglucosaminyltransferase (MGAT1ΔTM) to attach *N*-acetylglucosamine (GlcNAc) moiety on the α1,3 mannose of the Man3F(α1,3)F/Man3F. Next, α-1,6-mannosyl-glycoprotein 2-β-N-acetylglucosaminyltransferase (MGAT2ΔTM) was utilized to add GlcNAc to the α1,6 mannose, and eventually, β-N-acetylglucosaminylglycopeptide β-1,4-galactosyltransferase (β4GalT1ΔTM, further referred to as GalTΔTM) was employed to terminally galactosylate both antennas. This particular glycan remodelling strategy has previously succeeded on viral glycoproteins, namely, Spike protein of SARS-CoV-2 (Ruhnau et al., 2021), and hemagglutinin A of influenza A virus (pending publication),

produced in insect cell lines. Unlike previous attempts, where the recombinant human transmembrane domain-lacking (ΔTM) glycosyltransferases had been expressed in *E.coli*, their production this time was tested in insect cells to evaluate eukaryotic host suitability for routine production, and effect on the enzyme activity. By applying the outlined IVGE approach on Rituximab, the feasibility of novel monosaccharide-specific chemoenzymatic IVGE for insect cell-derived therapeutic mAb modulation was investigated, thus presenting a new outlook in IgG IVGE towards the ultimate S2(α2,6)G2 structure. By maintaining the entire workflow under chemically defined conditions, the applicability of reported approach in an industrial large-scale setup was assessed to support foundation of an IVGE platform for manipulation of therapeutic IgGs, and other therapeutic glycoproteins, in safe and regulated conditions.

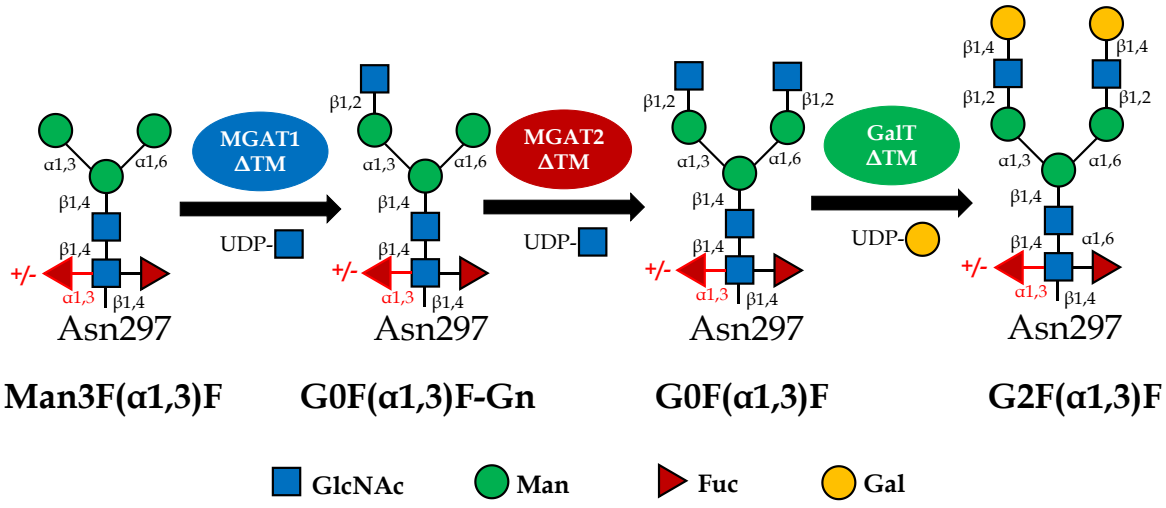

Figure 4. Novel IgG IVGE reaction cascade to obtain complex galactosylated *N*-glycoform from paucimannose insect cell glycans. Dominant *N*-glycan Man3(α1,3)F/Man3F (permanent presence of α1,6-linked core fucose, linkage not annotated for most glycoforms; varying presence of α1,3-linked core fucose, indicated by +/-) produced by insect cells on an antibody is developed into G0F(α1,3)F-Gn structure through β1,2 linking of UDP-GlcNAc to α1,3-mannose, catalyzed by MGAT1ΔTM. Through addition of UDP-GlcNAc to α1,6-mannose via MGAT2ΔTM activity, glycoform is modified into G0F(α1,3)F. Finally, both of the formed antennas are furnished with β1,4-galactose from UDP donor, attached by GalTΔTM. Illustrated structures represent *N*-glycans attached to position Asn297 of an intact Rituximab antibody. Activated monosaccharides are carried by a signaling molecule Uridine Diphosphate (UDP). GlcNAc corresponds to N-acetylglucosamine, Man to Mannose, Fuc to Fucose, Gal to Galactose. Unnatural to human glycosidic linkages are highlighted in red colour.

2 MATERIALS AND METHODS

2.1 Cell culture

Adherent *Spodoptera frugiperda* Sf9 (serum-free adapted) were obtained from Novagen Pharma (Pretoria, South Africa), and adherent BTI-TN-5B1-4 cell line derived from *Trichoplusia ni*, commercially known as HighFive™, was purchased from Thermo Fischer Scientific (Waltham, MA, U.S.A). Both cell lines were adapted to suspension format, and grown in serum-free chemically defined commercial medium. Sf9 cells were cultured without supplements in BacVector® medium (Merck, Burlington, MA, U.S.A), while HighFive™ were maintained in Express Five™ medium containing 18 mM L-Glutamine and 12.5 µg/ml Dextran Sulphate (from here onwards referred to as chemically defined complete culture medium (CDCCM)). For experiments, both Sf9 and HighFive™ cells that have not exceeded passage 50 were used; cells were cultured in the same media composition per each respective cell line as described for routine maintenance, unless stated otherwise. Both cell lines were passaged every three-four days, with seeding density of viable cell concentration (VCC) of 0.75×10^6 cells/ml for Sf9, and 0.30×10^6 cells/ml for HighFive™. Routine cell culture was maintained at 28 °C in a shaker-incubator without humidification and CO_2 supplementation, with mixing within 90-130 revolutions per minute (RPM) range, in flat-bottom glass and plastic shake flasks with vented cap. Cell density, viability, and diameter were determined with Vi-CELL XR (Beckman Coulter GmbH, Brea, CA, U.S.A). Culture plates, shake flasks, and miscellaneous materials were purchased from various manufacturers.

In small-scale cell culture experiments done in shake flasks, unless stated otherwise, cells were seeded into media with the same composition per each respective cell line as described for routine maintenance, and kept at the conditions identical to those applied for routine cell culture. Cell density, viability and diameter were determined daily with Vi-CELL XR. Once the cell viability reached or exceeded the threshold of 80%, or as specified, experiments were terminated.

2.2 Methods

2.2.1 Production of recombinant glycosyltransferases

2.2.1.1 Design of recombinant glycosyltransferases

The method of choice for generation of recombinant baculovirus (rBV) encoding *Homo sapiens* MGAT1, MGAT2, and GalT was homologous recombination in insect cells. Original sequences of the Leloir glycosyltransferases (Uniprot ID P26572 for MGAT1, Q10469 for MGAT2, and P15291 for GalT) were modified by removing transmembrane domain region (ΔTM) and introducing a polyhistidine

tag at the C-terminus of each enzyme. Further changes to the original sequences are not available for disclosure. Key characteristics of the employed enzymes are provided in Table 1. Optimized sequences were encoded into commercial monopromoter transfer vectors (mV) pOET8.VE1 (OET Ltd., Oxford, U.K.), constructed on the basis of *Autographa californica* multiple nucleopolyhedrovirus (AcMNPV) baculovirus, by BioCat GmbH (Heidelberg, Germany). Target gene sequences of each of the recombinant enzyme was placed under the control of polyhedrin (*polh*) promoter. Commercial AcMNPV baculoviral DNA *flash*BAC™ ULTRA was purchased from OET Ltd.

TABLE 1. Theoretical characteristics of recombinant glycosyltransferases MGAT1ΔTM, MGAT2ΔTM, and GalTΔTM employed in this study. Values were predicted with ProtParam tool (Expasy, Swiss Institute of Bioinformatics, Lausanne, Switzerland) based on amino acid sequences of the enzymes.

Enzyme	Number of amino acids	Theoretical molecular weight, kDa	Theoretical isoelectric point (pI)
MGAT1ΔTM	448	50.79	8.97
MGAT2ΔTM	450	51.47	8.52
GalTΔTM	424	46.62	8.49

2.2.1.2 Generation and primary amplification of rBV

rBV stocks P0 were generated according to the manufacturer's guidelines. 2 ml of 0.5×10^6 cells/ml Sf9 cell suspension in manufacturer-supplied Transfection medium were added per well of a 6-well plate and allowed to attach for 1 h. One well was reserved for one tested transfer vector construct. Virus DNA:transfer DNA complex was prepared by combining 100 ng of *flash*BAC™ ULTRA viral DNA, 500 ng of transfer DNA, and 1.2 µl of Lipofectamine™ Transfection Reagent (Thermo Fischer). After 20 min incubation, the complex was added to Sf9 cells with 1 ml of medium removed. The plate was incubated in static conditions overnight at 28 °C without CO_2 or humidification, with addition of 1 ml medium the next day to each well, and subsequent incubation in the same manner for 5 days until cells exhibited signs of cytopathic effect. Supernatant from each well was then harvested (P0) and immediately amplified in Sf9 cells.

For P0 amplification, Sf9 cells were seeded at the VCC of 2×10^6 cells/ml in shake flasks in a CDCCM without supplements, and infected with P0 stock at the time of seeding. Infected cells were grown in batch mode (no supplements added during cultivation) under standard conditions outlined for small-scale setup. Eventually, cells were removed by centrifugation at $2{,}000\times g$ for 10 min, and supernatant was aseptically collected and stored at -80 °C until further use. Both generation and P0 amplification of rBV were performed by project researcher Dr. Karim Jaén prior to the start of this Master thesis work. Resulting P1 stocks were used by the author of this thesis during practical training, carried out prior to the Master thesis work, and during the thesis work itself.

2.2.1.3 Large-scale secondary amplification of rBV stocks in bioreactor

P2 stocks were generated in large scale using 3 l stirred tank benchtop bioreactors BioFlo® 320 (Eppendorf, Hamburg, Germany) operated by DASware® control software (Eppendorf). The hardware configuration and setpoints of the bioreactor system are outlined in Table 2. In brief, bioreactors were inoculated with Sf9 cells to obtain VCC 0.5×10^6 cells/ml in working volume of 500 ml. The cells were grown until VCC of at least 4×10^6 cells/ml, at which they were infected with P1 rBV stock at multiplicity of infection (MOI) of 1×10^{-3} infectious particles per cell (IP/cell). At the time of infection, cells were supplemented with 10% chemically defined commercial feed solution HEK FS (Xell AG, Sartorius, Göttingen, Germany), and fresh CDCCM to reach the working volume of 1 l. Culture was maintained in batch mode until reaching the viability threshold of 80%. Cell suspension was centrifuged at 2,000×*g* for 10 min to remove cell debris, and the supernatant was harvested, clarified by peristaltic pump-assisted filtration through 0.22 µm Durapore® polyvinylidene fluoride (PVDF) membrane cassette Pellicon XL (Merck), and concentrated 5-10 times, ultrafiltrated, and buffer exchanged into 10 mM Tris (Carl Roth GmbH & Co. KG, Karlsruhe, Germany)-HCl (Carl Roth GmbH & Co. KG) pH 7.0, 150 mM NaCl (Carl Roth GmbH & Co. KG), 10% Trehalose Dihydrate (Merck) using tangential flow filtration through Vivaflow® 200 10,000 Da MWCO PES membrane cassette (Sartorius). Recovered filtrate containing baculovirus was stored at -80 °C.

TABLE 2. Hardware configuration and setpoints of Eppendorf BioFlo® 320 bioreactor system used for large-scale production on rBV encoding enzymes of interest.

Parameter	**Configuration**	**Growth phase**	**Infection phase**
		Setpoint	**Setpoint**
Vessel	3 l glass water-jacketed vessel	0.5 l working volume	1.0 l working volume
Gassing control	Thermal Mass Flow Controllers (TMFCs) with 0.04 – 20 SLPM flow range (Eppendorf)	No gas mixing	Automatic 2-Gas mix (air and oxygen)
Sparge	In-house spargers	3.0 Standard Litre Per Hour (SLPH) (macrosparger)	0.3 SLPH (microsparger)
Dissolved Oxygen (DO) control	ISM polarographic InPro® 6800 (Mettler Toledo, Columbus, OH, U.S.A)	50%	
Agitation	Elephant ear 3-blade impeller (Eppendorf)	100 RPM	
pH sensor	ISM gel-filled InPro 3253i pH sensor (Mettler Toledo)	none	
Temperature	N/A	28 °C	

2.2.1.4 Determination of infectious titre of rBV stocks

Virus titration and quantification was performed according to the protocol described by Mena et al. 2003. Sf9 cells were seeded at 1×10^5 viable cells/ml in 96-well flat-bottom plates in complete culture medium supplemented with 0.1% Gentamicin (Sigma Aldrich, St. Louis, MO, U.S.A) with final volume of 50 µl per well, and infected with 10 µl of serially diluted rBV stocks (from 10^{-1} to 10^{-11} dilution factor), 8 wells per each dilution. Infected cells were incubated for 12 days, after which to each well, 10 µl of 5 g/l 3-(4,5-Dimethylthiazol-2-yl)-2,5-Diphenyltetrazolium Bromide (MTT; Merck) solution was added. After subsequent 2 h incubation with mixing, plates were centrifuged at 2,000×*g* for 10 min, supernatant was removed, and the crystals were solubilized in 50 µl of Dimethyl Sulfoxide (DMSO; Merck). Absorbance of the purple formazan crystals was measured at 570 nm with Tecan Infinite ® M200 Pro Plate Reader (Tecan Life Sciences, Zürich, Switzerland). Obtained absorbance values were plotted against virus dilution, and the viable cell concentration curve was obtained by nonlinear curve fitting with *Growth/Sigmoidal* function category, and *Logistic* function, represented by Equation 1, in OriginPro (OriginLab Corporation, Northampton, MA, U.S.A). From the obtained x_0 value, median tissue culture lethal dose $TCLD_{50}$/ml was calculated using Equation 2, and from this value, log$TCID_{50}$/ml (median tissue culture infectious dose) was calculated using Equation 3; both Equation 2 and 3 are presented in the reference protocol. Equation 4 was then applied to convert resulting values into $TCID_{50}$/ml, which represents the infectious titre of the baculovirus stock.

Equations:

$$y = \frac{A_1 - A_2}{1 + \left(\frac{x}{x_0}\right)^p} + A_2, \quad (1)$$

where y is absorbance at 570 nm, A_1 is the maximum absorbance (0% of response, maximum VCC detected), A_2 is the minimum absorbance (100% of response, minimum VCC detected), x is viral dilution, x_0 is viral dilution at which response was 50% ($1/TCLD_{50}$), p is the slope factor;

$$TCLD_{50}/mL = \frac{1}{x_0 V}, \quad (2)$$

where V is the volume of diluted virus per each well (0.010 ml);

$$\frac{logTCLD_{50}}{mL} = 0.912\left(\frac{logTCLD_{50}}{mL}\right) + 1.674, \quad (3)$$

where *0.912* and *1.674* are experimentally determined values from original protocol.

$$TCID_{50}/mL = 10^{logTCID_{50}/mL}, \quad (4)$$

2.2.1.5 Purification and concentration of rBV stocks with steric exclusion chromatography (SXC)

SXC with dynamic light scattering (DLS) was performed according to the protocol by Marichal-Gallardo et al. 2021. Experiments were done with ÄKTApure purification system (Cytiva, Marlborough, MA, U.S.A) coupled to NICOMP® 380 Submicron particle sizer (Particle Sizing Systems, Orlando, FL, U.S.A). From supernatant collected after P1 baculovirus amplification, virus was isolated by centrifugation at 2,000×*g* for 10 min, and injected into chromatographic system, where in-line mixing with binding buffer (1×PBS containing 16% polyethylene glycol of molecular weight 6000 Da (PEG-6000); Merck) was done. The column, made out of regenerated cellulose membranes with pore size 1.0 µm (Whatman, Maidstone, U.K.), was assembled according to the instructions provided in the original protocol. Wash step was performed with in-line mixing of binding and wash buffer (1×PBS), and virus particles were eluted using 1×PBS supplemented with 300 mM NaCl. Collected fractions were dialyzed overnight in buffer containing 10 mM Tris-HCl pH 7.0, 150 mM NaCl, 10% Trehalose Dihydrate, filtered through 0.22 µm PES syringe filters (Merck), and stored at -80 °C until use.

2.2.1.6 Expression of recombinant enzymes

HighFive™ cells were seeded at an experimentally determined optimal seeding density in shake flasks and immediately infected with P1 stock at an experimentally determined optimal MOI condition (details are provided in Background material Section 1.1). At least one flask cultured at tested conditions was kept as uninfected negative control. Upon reaching the viability threshold, cell suspension was centrifuged at 2,000×g for 10 min, supernatant was discarded, and cell pellet was either immediately processed for enzyme extraction and purification, or stored dry at -80 °C until further use. To monitor intracellular enzyme expression rate during cultivation, 2×10^5 infected cells were collected every 24 hours, centrifuged at 2,000×*g* for 10 min, and stored dry at -80 °C.

2.2.1.7 Enzyme assessment with SDS-PAGE and Western blot

For both SDS-PAGE and Western blot, samples were 1:2 diluted in Sample buffer containing 65.8 mM Tris-HCl pH 6.8, 26.3% (v/v) Glycerol (Carl Roth GmbH & Co. KG), 2.1% (w/v) SDS (Merck), 0.01% (w/v) Bromophenol Blue (Merck), and 5% β-mercaptoethanol (βME; Sigma Aldrich), denatured by boiling at 95° C for 10 min, and separated in 10% Mini-PROTEAN®TGX™ Tris/Glycine/SDS Precast gels (12- and 15-well) (Bio-Rad, Hercules, CA, U.S.A) at 150 V for 1 h in 25 mM Tris, 192 mM Glycine, 0.1% (w/v) SDS, pH 8.3 Running buffer (Bio-Rad). Gels were stained for 1 h at gentle agitation in Staining solution containing 0.1% (w/v) Coomassie Brilliant Blue R 250 (Merck), 10% Acetic acid glacial (Carl Roth GmbH & Co. KG), 30% Ethanol (Carl Roth GmbH & Co. KG), 60% MilliQ H_2O; destaining was done under the same conditions in solution of identical composition without Brilliant Blue. For investigation of intracellular expression

rate of the recombinant enzymes, frozen samples containing 2×10^5 cells, collected during expression experiments, were reconstituted in 100 µl 1×PBS, and 20 µl of resulting suspension were mixed in 1:1 ratio with Sample buffer; 10 µl of the denatured sample mixture containing 1×10^4 cells were loaded per well for both SDS-PAGE and Western blot analyses. Molecular weight marker PageRuler™ Plus Prestained Protein Ladder #26619 (Thermo Scientific) was used for both SDS-PAGE and Western blot. In chemiluminescent Western blot, protein separation by gel electrophoresis was followed by protein transfer from gel to 0.45 µm PVDF membrane using electroblotting (100 V; 1 h) in 25 mM Tris, 192 mM Glycine, 20% (v/v) Methanol buffer. Electrophoretic transfer was performed in Mini Trans-Blot® Cell (Bio-Rad). The membranes were blocked in TBST (20 mM Tris-HCl pH 7.6, 137 mM NaCl, 0.1% Tween 20 (Sigma Aldrich)) with 5% Milk powder (Carl Roth GmbH & Co. KG) (TBSTM) for 2 h at room temperature and gentle agitation, or overnight at +4 °C. Enzymes were labelled with monoclonal anti-His tag primary antibody from mouse (Sigma-Aldrich) diluted 1:1,000 in TBSTM during 1 h incubation, followed by anti-Mouse, horse radish peroxidase (HRP)-conjugated secondary antibody from sheep (Sigma Aldrich) diluted to 1:5,000 in TBSTM during 1 h incubation. After extensive washing in TBST, chemiluminescent signal from the detected enzymes was generated using SuperSignal™ West Femto kit (Themo Scientific), and detected with Intas ECL Chemostar (Intas Science Imaging GmbH, Göttingen, Germany).

2.2.1.8 Enzyme purification using immobilized metal affinity chromatography (IMAC)

HighFive™ cell pellets obtained from expression experiments were lysed using experimentally determined optimal lysis buffer and lysis method (details are provided in Background material Section 1.1) In experiments aimed at optimization of lysis method and buffer composition, purification was performed at small scale with His SpinTrap TALON® (Cytiva) spin columns following the manufacturer's protocol. In large-scale purifications, extracted enzymes were applied to ÄKTApure purification system (Cytiva) equipped with Co^{2+}-NTA HiTrap TALON® crude 1 ml column (Cytiva). Finalized buffer compositions for each step of IMAC procedure are provided in Background material Section 1.1. Recovered elution fractions were concentrated using Amicon® Ultra Centrifugal Filter Devices with 10,000-30,000 Da molecular weight cut-off (MWCO) membranes (Merck), and buffer-exchanged with same filter devices into optimal buffer composition. Concentrated eluates were stored in 50% Glycerol at -20 °C until further use.

2.2.1.9 Enzyme quantification with bicinchoninic acid (BCA) total protein assay

Total protein in fractions obtained from IMAC purification of enzymes was quantified with BCA assay using Pierce™ BCA Protein Assay Kit (Thermo Scientific) according to the kit instructions. In short, protein samples of interest were diluted to an assumed concentration of up to 2 mg/ml, and 25 µl of the final

solution were added per well of a 96-well plate. Provided Pierce Dilution-Free BSA Protein Standards were plated in the same manner, and both samples and standards were quantified in either biological duplicates or triplicates. Bicinchoninic acid solution was prepared by combining provided Reagent A and Reagent B in ratio 50:1 A:B (v/v), from which 200 µl were added per each well of a 96-well plate corresponding to a sample and a standard. 96-well plate was then incubated for 30 min at 37 °C without mixing, and absorbance was measured at 562 nm using Tecan Infinite ® M200 Pro Plate Reader (Tecan Life Sciences). Absorbance data was analysed in Microsoft Excel (Microsoft Corporation, Redmond, WA, U.S.A) using scatter plot and linear regression model for standard curve fitting.

2.2.1.10 Enzyme conversion activity assessment

The activity of the enzymes was tested in a cell-free reactions containing mixture of produced enzyme, activated sugar, and free *N*-glycan precursor in a buffer of choice. For each enzyme, a range of concentrations was tested to find the optimal value based on the resulting conversion rate. Each reaction contained a single enzyme at a specific concentration; range of tested concentrations was determined by the enzyme stock concentrations. Commercial precursors AdvanceBio Man3F/FM3 Standard and AdvanceBio APTS G0F/FA2 Standard (Agilent Technologies, Santa Clara, California, U.S.A) were used for MGAT1ΔTM and GalTΔTM reactions, and G0F-Gn precursor for MGAT2ΔTM reactions was derived from a completed MGAT1ΔTM reaction. Final volume of each reaction constituted 10 µl. Further details on the buffer choice and reaction conditions are provided in Background material Section 1.1. Products of the reactions were processed and assessed with multiplexed capillary gel electrophoresis with laser induced fluorescence detection (xCGE-LIF) as described in Section 2.2.3.3. Prior to xCGE-LIF assessment, products of reactions containing AdvanceBio APTS G0F/FA2 Standard as the starting *N*-glycan substrate were labelled with fluorescent dye as described in Section 2.2.3.2.

2.2.2 Production of monoclonal antibody Rituximab

2.2.2.1 Vector design for antibody expression using rBV

Two types of commercial transfer vectors applicable for generation of rBV in insect cells through homologous recombination were used. In the first type, a dual promoter AcMNPV baculovirus transfer vector (dV) pOET5.1 (OET Ltd., Oxford, U.K.) was used to encode both light and heavy chains of Rituximab in a single vector: light chain sequence was placed downstream of *p10* promoter, while heavy chain was under control of the *polh* promoter. In the second approach, a monopromoter baculovirus transfer vector pOET8.VE1 (OET Ltd.) was used to express either light or heavy chain of Rituximab under AcMNPV baculovirus *polh* promoter. Sequences of light (LC) and heavy chain (HC) in each transfer vector type were supplemented with Kozak sequence. Maps of the

transfer vectors are provided in Appendix 1. Commercial AcMNPV baculoviral DNA *flash*BAC™ ULTRA was purchased from OET Ltd.

2.2.2.2 Generation and primary amplification of rBV encoding Rituximab

rBV encoding each of the Rituximab chain / chain combination (dV: LC and HC; mV: LC/HC) were generated in the same manner as described for the enzymes, resulting in three primary stocks P0, one per each transfer vector. P0 was immediately amplified into P1 using amplification protocol described for the enzymes. Resulting baculovirus P1 stocks were stored at -80 °C until further use. P2 stocks for each transfer vector construct were produced in small-scale, using P1 for infecting cells at MOI 1×10^{-3} IP/cells until cell viability threshold was exceeded. Unlike P1 stocks, P2 were not purified or concentrated using SXC, and were directly stored at -80 °C. Baculovirus titre for each stock was quantified as described in Section 2.2.1.2.

2.2.2.3 Small-scale expression of Rituximab

Expression experiments were performed in both batch and fed-batch modes, the latter including regular addition of nutrient substrate. In both modes in all experiments, at least one uninfected flask was cultured at tested conditions serving as negative control. For batch experiments, HighFive™ cells were seeded at the VCC of 2×10^6 cells/ml in shake flasks in a CDCCM, and immediately infected with P1 or P2 stock at the MOI of either 1, 5, or 10 IP/cell. dV P1 and P2 stocks were added directly in the amount that corresponded to the target MOI. Baculovirus stocks for LC and HC of Rituximab, obtained from mV, were added in one of three ratios per each expression variant: 1:1 LC:HC; 1.5:1 LC:HC, 2:1 LC:HC. Cultivation was performed under standard conditions for small-scale expression experiments. The cell suspension at viability of 80% or lower was centrifuged at 2,000×*g* for 10 min, cell pellet and debris were discarded, and the supernatant was either immediately processed for antibody capture and purification, or stored at –80 °C until further use. To evaluate antibody expression rate during cultivation, 500 µl supernatant samples (extracellular expression) and 2×10^5 cells (intracellular expression) were collected every 24 h; samples were centrifuged at 2,000×*g* for 10 min. Both intracellular and extracellular fractions were stored at -80° C until analysis. Additionally, 10 ml of 0.22 µm PES syringe filtered (Merck) supernatant was preserved for evaluation with SDS-PAGE and Western blot.

For fed-batch experiments, HighFive™ cells were seeded at the VCC of 2×10^6 cells/ml in shake flasks in CDCCM either without supplements, or with 75 mM Trehalose, and immediately infected with P2 stock at the MOI of 20 IP/cell. Depending on the fed-batch strategy employed, cells were supplemented with Trehalose, commercial chemically defined feeding supplement HEK FS. On day 3, all variants were supplemented with L-Glutamine (Merck), and selected variants were supplemented with L-Cysteine hydrochloride monohydrate (Sigma Aldrich), after which all variants were cultured at 20 °C until the end of

the experiments. Two tested feeding supplement strategies for small-scale expression are outlined in Table 3. Cultivation was performed under conditions identical to those described for small-scale expression experiments until cell viability of 80% or lower was reached, or viability rapidly dropped ≥ 10%. The cell suspension was then centrifuged at 2,000×*g* for 10 min, cell pellet and debris were discarded, and the supernatant was either immediately processed for antibody capture and purification, or stored at -80 °C until further use. Sampling for evaluation of intracellular and extracellular expression rates of the antibody during cultivation was done in the same manner as for batch experiments.

TABLE 3. Feeding strategies implemented in small-scale expression experiments for Rituximab production in baculovirus-infected insect cells.

Day of cultivation	**Supplement**	**Feeding strategy 1**	**Feeding strategy 2**
		Final concentration	**Final concentration**
0	HEK FS	0%	5%
	+ /- Trehalose in medium	75/0 mM	75/0 mM
1	HEK FS	3%	-
2	HEK FS	6%	5%
3	HEK FS	10%	-
	L-Glutamine	18 mM	
	+ /- L-Cysteine	130 /0 µM	
	N/A	Temperature shift 28 → 20 °C	
4	HEK FS	10%	10%
5	HEK FS	12%	-
6	HEK FS	-	-

2.2.2.4 Large-scale expression of Rituximab

Rituximab was expressed in two 3 l benchtop bioreactors BioFlo® 320 operated by DASware® control software (both by Eppendorf). The hardware configuration and setpoints of the bioreactor system were identical to those presented for large-scale baculovirus amplification (Table 2), except for working volume during both growth phase and infection phase (0.5 l/bioreactor). In brief, one of the bioreactors was inoculated with HighFive™ cells to obtain VCC 0.3×10^6 cells/ml in working volume of 500 ml. The cells were seeded and grown in CDCCM without supplements until VCC of around 4×10^6 cells/ml, at which cell suspension was split equally between two bioreactors through sterile tubing, operated by peristaltic pump, to obtain 250 ml of suspension in each bioreactor. Each vessel then was infected with P2 rBV dV stock at MOI of 1 IP/cell (Unit 1) and 0.1 IP/cell (Unit 2) for target working volume of 500 ml. At the point of infection, cells were supplemented with 10% HEK FS and fresh CDCCM to reach the working volume per each unit. Infected HighFive™ were cultured in fed-batch mode using feeding strategy 1, explained in previous subsection, without Trehalose and supplements added at day 3 (L-Glutamine, L-Cysteine), as well as

without temperature shift. Cells were cultivated until displaying stagnation of VCC, or VCC decline. The suspension from each unit was then centrifuged at 2,000×*g* for 10 min to remove cell debris, and the supernatant was harvested, clarified by peristaltic pump-assisted tangential flow filtration through 0.22 µm Durapore® PVDF membrane cassette Pellicon XL, and concentrated 5-10 times, diafiltrated into 1×PBS using tangential flow filtration through Vivaflow® 200 30,000 Da MWCO PES membrane cassette. Recovered retentate from each unit was immediately processed with liquid chromatography.

2.2.2.5 Rituximab purification using Protein G affinity chromatography

Clarified and concentrated HighFive™ supernatants were directly applied to HiTrap™ Protein G HP 1 ml column (Cytiva) equilibrated in 1×PBS, operated on ÄKTApure (Cytiva). Bound Rituximab was eluted using 0.1 M Glycine-HCl pH 3.0. For purification of bioreactor-produced antibody, four-step elution protocol was applied, where concentration of elution buffer was set at 25, 50, 75, and 100% per step, with each step lasting for 5 column volumes (CV). For enhanced antibody detection, UV absorbance at 220 nm was monitored during large-scale product processing alongside standard absorbance at 280 nm. Collected eluate was neutralized to approximate pH 7.0 using 1 M Tris pH 10.5, after which it was concentrated and rebuffered to 1×PBS using Amicon® Ultra Centrifugal Filter Devices with 10,000-30,000 Da MWCO membranes. Quantification of protein content was performed with NanoDrop ND-1000 (Thermo Fischer) by measuring absorbance at 280 nm, with automatic correction using IgG extinction coefficient. Purified fractions were stored either at +4 or -20 °C.

2.2.2.6 Rituximab assessment with SDS-PAGE and Western blot

For both SDS-PAGE and Western blot, samples were prepared either in reducing or non-reducing conditions. Non-reduced samples were 1:2 diluted in Sample buffer containing 65.8 mM Tris-HCl pH 6.8, 26.3% Glycerol, 2.1% (w/v) SDS, 0.01% (w/v) Bromophenol Blue, and denatured by boiling at 95 °C for 10 min. Reduced samples were prepared in the identical manner using Sample buffer supplemented either with 5% βME, or with 20 mM Dithiothreitol (DTT; Merck); for the latter, samples were incubated at 37 °C for 30 min prior to denaturing. Alongside all antibody samples, a reference Rituximab molecule was loaded into the gels. The reference clinical-grade antibody from the original Mabthera® commercial drug was purchased from Evidentic GmbH (Berlin, Germany).

For investigation of intracellular expression rate of Rituximab, the same procedure as one described for enzymes was applied (Section 2.2.1.7). For extracellular studies, 500 µl supernatants were dried for at least 3 h using rotational vacuum concentrator SpeedVac RVC 2-33 CDplus (Martin Christ Gefriertrocknungsanlagen GmbH, Osterode am Harz, Germany), and reconstituted in 50 µl of MilliQ H_2O, after which 20 µl were mixed with the Sample buffer of suitable composition; further steps were identical to those previously outlined for the enzymes. 10 ml samples of clarified supernatant

harvest collected from small-scale batch and fed-batch experiments were concentrated 10 times using Amicon® Ultra Centrifugal Filter Devices with 10,000-30,000 Da MWCO membranes before following the same procedure for electrophoretic analysis. SDS-PAGE and Western blot setups for reduced and non-reduced antibody samples were identical to those described for the enzymes. In Westen blot, antibody was labelled using only secondary Goat anti-Human IgG F(ab')2:HRP antibody (Bio-Rad) with 1:5,000 dilution in TBSTM.

2.2.3 IVGE of Rituximab

2.2.3.1 Design of IVGE reaction cascade

The 3-enzyme cell-free reaction cascade was designed on the basis of previously reported IVGE approach for Spike protein (Ruhnau et al. 2021) and currently unpublished setup for hemagglutinin A. In general, 45 µg of produced Rituximab species were immobilized on protein A magnetic beads, to which a reaction mixture containing one recombinant enzyme, activated sugar (purchased from Sigma Aldrich; UDP-GlcNAc for both MGAT1ΔTM and MGAT2ΔTM; UDP-Gal for GalTΔTM), and reaction buffer, were added for an incubation, after which reaction mixture was discarded and replaced with a fresh one containing next-in-cascade enzyme. Between each reaction mixture, immobilized antibody material was washed with reaction buffer. Exact setup with specific details is provided in Background material section 1.2.

2.2.3.2 Rituximab preparation for *N*-glycan analysis

For *N*-glycoprofile analysis of original and glycoengineered antibody, glycans were first released from the antibody, labelled with fluorescent dye, and cleaned using liquid chromatography. Rituximab preparation was performed using protocol described by Wiśniewski et al., 2009. In short, 7-10 µg of antibody in Pall® Nanosep™ Centrifugal Filtration Device with 30,000 Da MWCO (Pall Corporation, NY, U.S.A) were denatured by washing in 8 M Urea (Carl Roth GmbH + Co. KG) in [0.1 M Tris-HCl pH 8.5] buffer, reduced with 40 mM DTT in [0.1 M Tris-HCl pH 8.5, 8 M Urea] buffer during incubation at 56 °C for 20 min with gentle agitation, and alkylated with 55 mM Iodoacetamide (IAA; Merck) in [50 mM NH_4HCO_3 (Carl Roth GmbH + Co. KG)] buffer during 20 min incubation. Antibody was then digested into peptides by incubation with Proteinase K (New England Biolabs, Ipswich, MA, U.S.A), with enzyme:substrate ratio 1:20, in buffer [50 mM NH_4HCO_3, 5% Acetonitrile (ACN; Merck), 1 mM $CaCl_2$ (Carl Roth GmbH + Co. KG)], overnight at 37 °C and gentle agitation. Deglycosylation was achieved by PNGase A (New England Biolabs) digestion using 2 µl of 5,000 Unit/ml enzyme solution per peptides obtained from 10 µg of Rituximab, with addition of 2 µl of 10×Glycobuffer 3 (New England Biolabs) and 16 µl of MilliQ H_2O. After 24 h incubation at 37 °C and gentle agitation, reaction mixture was evaporated in rotational evaporator SpeedVac RVC 2-33 CDplus.

Next, *N*-glycan samples were labelled with 8-aminopyrene-1,3,6-trisulfonic acid (APTS; glyXera, Magdeburg, Germany). In short, dried *N*-glycans were reconstituted in 2 µl MilliQ H_2O, and incubated in solution containing 2 µl APTS and 2 µl ReduX Solution from glyXprep™ Glycan Labeling Kit (glyXera) for 3 h at 37 °C. After labelling, hydrophilic interaction liquid chromatography-solid phase extraction (HILIC-SPE) cleanup was performed to remove excess APTS, salts, and other impurities. For this, polyacrylamide beads Bio-Gel P-10 (Bio-Rad) were loaded into wells of Pall® AcroPrep™ 96-well filter plate (Pall Corporation), coupled to a vacuum manifold. All purification steps were performed with vacuum assistance. Equilibration of the column material in filter plate wells was done using 80:20% (v/v) ACN-water solution, after which APTS-labelled samples were loaded. Washing of the samples was carried out in 80:20% (v/v) ACN-water solution containing 100 mM triethylamine (TEA; Merck), followed by 80:20% (v/v) ACN-water solution. Purified labelled *N*-glycans were eluted with water, dried with rotational evaporator, and reconstituted in 10 µl MilliQ H_2O.

2.2.3.3 *N*-glycoprofile analysis

N-glycoprofile fingerprinting was done by multiplexed capillary gel electrophoresis with laser induced fluorescence detection (xCGE-LIF). 1 µl of 1:100 diluted in MilliQ H_2O purified labelled *N*-glycan sample was mixed with 0.5 µl GeneScan™ 500 LIZ® Size standard (Applied Biosystems, Thermo Fischer) diluted 1:50 in Hi-Di™ Formamide (Thermo Fischer), 0.5 µl 2nd Norm MiX sample alignment standard (glyXera), and 10 µl Hi-Di™ Formamide. Resulting solution was loaded into wells of 384-well microplate, and run in 3130 Genetic Analyzer (Applied Biosystems) using in-house developed protocols. Glycoform analysis was performed with glyXboxCE™-system (glyXera). Data processing, normalization of migration times, and annotation of *N*-glycan fingerprints were performed with glyXtool™ software (glyXera) version 11.3, and electropherogram plotting was done in OriginPro (OriginLab Corporation).

3 RESULTS

3.1 Production of recombinant glycosyltransferases

The work on production of recombinant glycosyltransferases MGAT1ΔTM, MGAT2ΔTM, and GalTΔTM in insect cells had started prior to initiation of this Master thesis project. Already generated (P0) and amplified (P1) rBV stocks, encoding each of the target enzymes, had been used during practical training, preceding Master thesis work, to establish expression and purification protocols (Figure 5). For expression procedure establishment, suspension cell lines Sf9 and HighFive™ were infected at various MOI conditions with P1 stocks to determine an optimal host based on intracellular enzyme expression rate. According to SDS-

PAGE and Western blot assessment, HighFive™ infected at high MOI demonstrated expression rate superior to that of Sf9 cells (GalTΔTM data provided as example in Figure 5A). The latter only sustained low infectious dose without exceeding viability threshold of 80% by 72 hours post infection (hpi) (data not shown). Western blot analysis of enzyme expression rate over the course of infection has shown that target enzymes were synthesized as early as 24 hpi in HighFive™, and as late as 72 hpi in Sf9 under investigated conditions. Thus, for further experiments, HighFive™ was chosen for infection using high doses of rBV stocks. When the first attempts to extract and purify enzymes from HighFive™ cell lysates were performed, no enzyme detected in the intracellular fraction of cell suspension (S; Figure 5B) was recovered in elution (E; Figure 5B), according to SDS-PAGE analysis. An extensive screening of lysis approaches, liquid chromatography methods, and buffer compositions was performed in small scale on cell pellets containing MGAT2ΔTM and GalTΔTM in order to enhance enzyme recovery in eluate (results for MGAT2ΔTM demonstrated in Figure 5B). An optimized protocol with gentle lysis approach and best-performing IMAC buffer composition yielded partial enzyme presence in the eluate (Figure 5B), with significant share of MGAT2ΔTM content in insoluble fraction (debris; D in Figure 5B). This protocol was then tested in large scale for purification of all three enzymes and establishment of enzyme stocks, and achieved very low recovery of MGAT1ΔTM and MGAT2ΔTM, but sufficient yield of GalTΔTM. The yields were the following: MGAT1ΔTM: 0.14 mg/L; MGAT2ΔTM: 0.52 mg/L, GalTΔTM: 1.57 mg/L (Table 4). Conversion activity of each obtained enzyme stock was confirmed on free glycans (data not shown). These investigations concluded the practical training work.

In the thesis project timeline, an additional cell lysis and IMAC buffer optimization was implemented to further improve enzyme recovery, with focus on MGAT1ΔTM and MGAT2ΔTM (Figure 6). Two buffer formulation approaches were investigated in small scale purifications on MGAT1ΔTM cell pellet – additives that stabilize protein structure (Figure 6A: conditions 1-3), and additives that solubilize protein structure without denaturation (conditions 4-5). Stabilizing additives Trehalose (condition 2) and Mannitol (condition 3) were used based on their proven performance in protein recovery (Leibly et al. 2012) in concentrations tested by the authors of the study – 750 mM Trehalose and 500 mM Mannitol in lysis buffers, and 5% (w/v) in binding buffer. Additionally, effect of glycosyltransferase cofactor Mn^{2+} in lysis and binding buffers (10 mM $MnCl_2$ in both) was investigated (condition 1). SDS-PAGE analysis of the original cell suspension in corresponding lysis buffer (S) and eluates of tested conditions (E) identified that the best MGAT1ΔTM recovery rate was achieved with solubilization additives (condition 4 and 5) (Figure 6A). Solubilizer from condition 4 was used to verify the protocol in large-scale purification using HighFive™ lysate obtained from 40 ml of infected cell suspension expressing MGAT1ΔTM (Figure 6B). The position and composition of protein bands obtained in the SDS-PAGE of the large-scale run appeared much different to those observed in small-scale test. An assumption from the final SDS-PAGE was

drawn that the eluate contained protein bands in the molecular weight (MW) region expected for MGAT1ΔTM, however, recovery rate demonstrated in large scale was inferior to that in small scale. A re-test, and a more advanced assessment of cell lysis and IMAC buffer parameters was thus required. To perform that, more cells expressing target enzymes were needed.

To generate more material for optimization experiments, large-scale amplification of rBV stocks encoding MGAT1ΔTM and MGAT2ΔTM was performed in bioreactors. During the entire production process, dynamics of key parameters of the culture (viable cell density (VCC) and viability, Dissolved Oxygen (DO) and pH) indicated successful progression of the experiment (Figure 7A,B). For both MGAT1ΔTM and MGAT2ΔTM producing bioreactors, growth phase (-96 to 0 hpi) was characterized by exponential growth rate, achieving VCC of just below 6×10^6 cells/ml by the start of infection phase (0-48 hpi). DO concentration decreased steadily for both units from the moment of bioreactor seeding, but did not drop below 50% threshold. pH demonstrated similar trend, with values remaining in the 5.9–6.2 range. At the moment of infection, cell suspension in both units was diluted approximately 1:2, resulting in VCC of around 3×10^6 cells/ml at 0 hpi, which dropped insignificantly at 24 hpi, yet started to recover by the harvest timepoint (48 hpi). During infection period, both DO concentration and pH remained relatively stable. Notably, both VCC and viability trends of both bioreactors during infection were rather similar to those observed in small-scale rBV amplification in shake flasks (data not shown). The most deviating behaviour was observed in cell diameter values, which were within 16.0-16.5 µm during growth phase of both bioreactor units, but decreased upon infection (for MGAT2ΔTM), or at 24 hpi (for MGAT1ΔTM). In small-scale amplifications, Sf9 cell diameter progressively increased from 15-16 µm towards 18-20 µm during baculovirus infection until cell viability decrease below 80% (data not shown). In the large-scale amplification, cell viability during infection for both MGAT1ΔTM and MGAT2ΔTM infected bioreactors remained above 80% (MGAT1ΔTM unit reached 85%, MGAT2ΔTM stayed at 90% by the time of harvest), hence the diameter decrease was not associated with the decline of the infected cultures. MTT assay of serially diluted rBV P2 product from bioreactors revealed high cell viability in all infected wells of 96-well plates for both MGAT1ΔTM and MGAT2ΔTM, represented by high amount of purple formazan salts produced by metabolically active Sf9 cells (Figure 7C). Reference titration plates of high-titre rBV P1 stocks produced in shake flasks were typically characterized by absence of purple formazan crystals in columns 1-6 following cell death induced by high concentrations of infection-potent baculovirus. Consistent presence of formazan salts in all columns of titration plates with bioreactor-produced P2 stocks indicated low baculovirus infectivity, and therefore virus titre was not quantified, and the P2 stocks were deemed not applicable for expression experiments.

Due to the unsuccessful amplification of MGAT1ΔTM and MGAT2ΔTM rBV in bioreactors, and exhaustion of previous shake-flask produced P1 stocks for each enzyme, required expression experiments for production of enzymes in

insect cells were not performed in the thesis project timeline. In IVGE reactions, first established enzyme stocks were utilized, however, due to low concentrations of enzymes, the same three recombinant glycosyltransferases were produced in *E.coli* by Dr. Karim Jaén, and were used alongside insect-cell derived products in IVGE studies. The yields in *E.coli*-based production were the following: MGAT1ΔTM: 1.18 mg/L; MGAT2ΔTM: 0.41 mg/L; GalTΔTM: 0.50 mg/L (Table 4); purity of each *E.coli*-derived enzyme stock was estimated to be roughly 50%, according to SDS-PAGE analysis (data not shown).

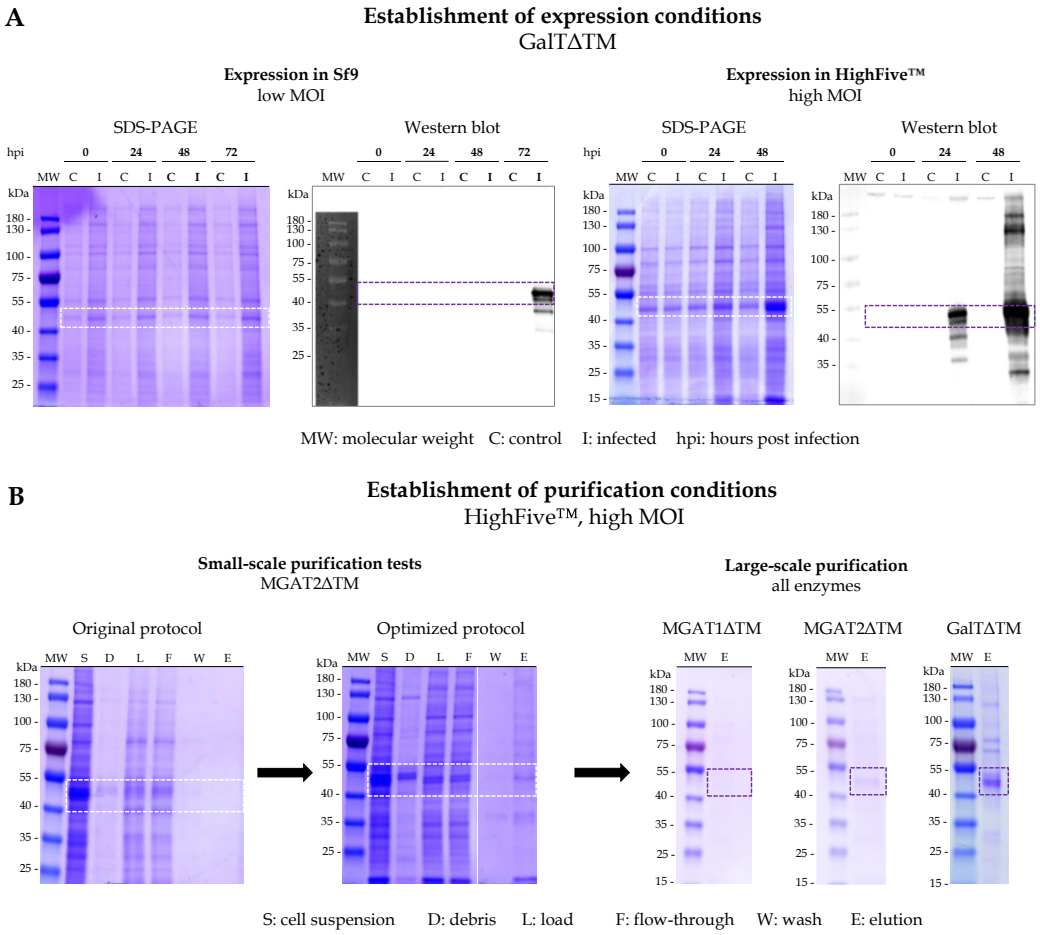

Figure 5. Key results determining the setup for expression and purification of recombinant glycosyltransferases. **A) Establishment of expression conditions:** SDS-PAGE and Western blot results obtained for GalTΔTM represent the kinetics of intracellular expression rate of the enzyme in Sf9 or HighFive™ cells infected with rBV. MW shows pre-stained protein ladder; C represents uninfected control; I stands for infected cells. Duration of infection is shown in hours post infection (hpi). **B) Establishment of purification conditions:** SDS-PAGE of lysates from HighFive™ cells infected at high MOI, processed in small- and large-scale IMAC setups to determine suitable purification protocol. For small-scale attempts, only results for MGAT2ΔTM are shown. In all gels, dashed purple or white figures highlight the region of theoretical MW of the enzymes.

TABLE 4. Evaluation of working stocks of recombinant Leloir glycosyltransferases MGAT1ΔTM, MGAT2ΔTM, and GalTΔTM, produced in two expression hosts, prokaryotic (*E.coli*) and eukaryotic (Lepidopteran insect cells HighFive™). Yield is represented as mean of three values with standard deviation (SD).

Expression host	Cell line/strain	Enzyme	Yield, mg/L	Purity, %
Prokaryotic	*E.coli* BL21(DE3)	MGAT1ΔTM	1.18 (± 0.07 SD)	~50
		MGAT2ΔTM	0.41 (± 0.04 SD)	
		GalTΔTM	0.50 (± 0.09 SD)	
Eukaryotic	HighFive™	MGAT1ΔTM	0.14 (± 0.05 SD)	~50
		MGAT2ΔTM	0.52 (± 0.02 SD)	
		GalTΔTM	1.57 (± 0.11 SD)	

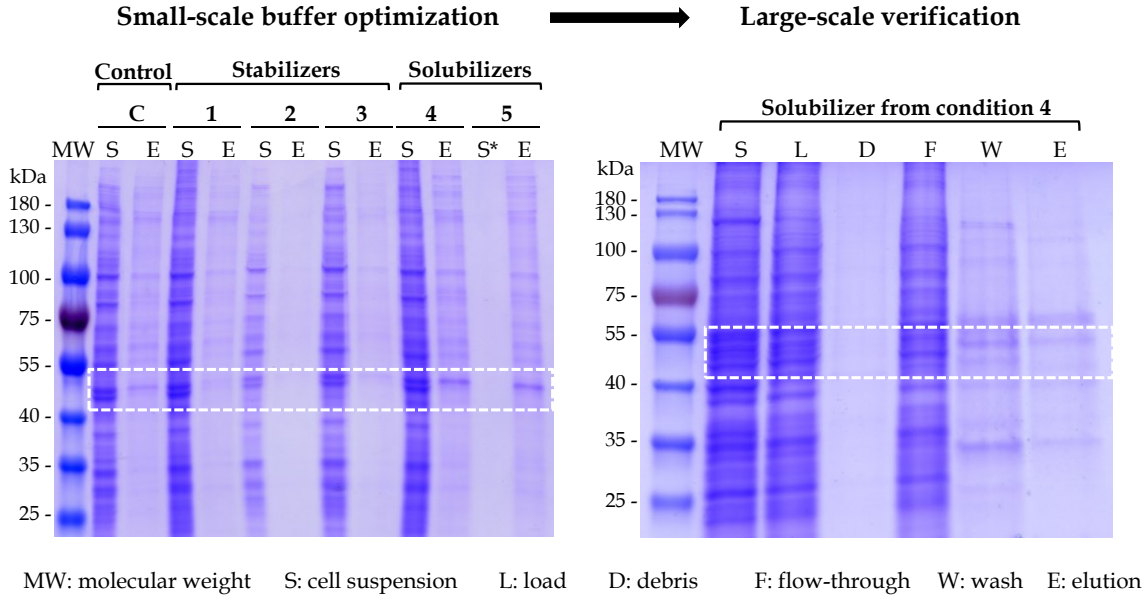

Figure 6. SDS-PAGE of IMAC runs in small and large scale aimed at optimization of recombinant enzyme recovery from HighFive™ cells. Results for MGAT1ΔTM are shown. In small-scale IMAC run, SDS-PAGE gel only contained samples of cell suspension (S) in lysis buffer of tested formulation, and resulting elution (E). Each tested condition corresponding to unique number formulation is labelled from 1-5, with C representing control formulation. S* for condition 5 showed no protein bands in the well, most likely due to human error. Small-scale optimization was run in 10% gel, while large-scale samples were loaded into 12% gel. Dashed white figures highlight the region of theoretical MW of the enzymes.

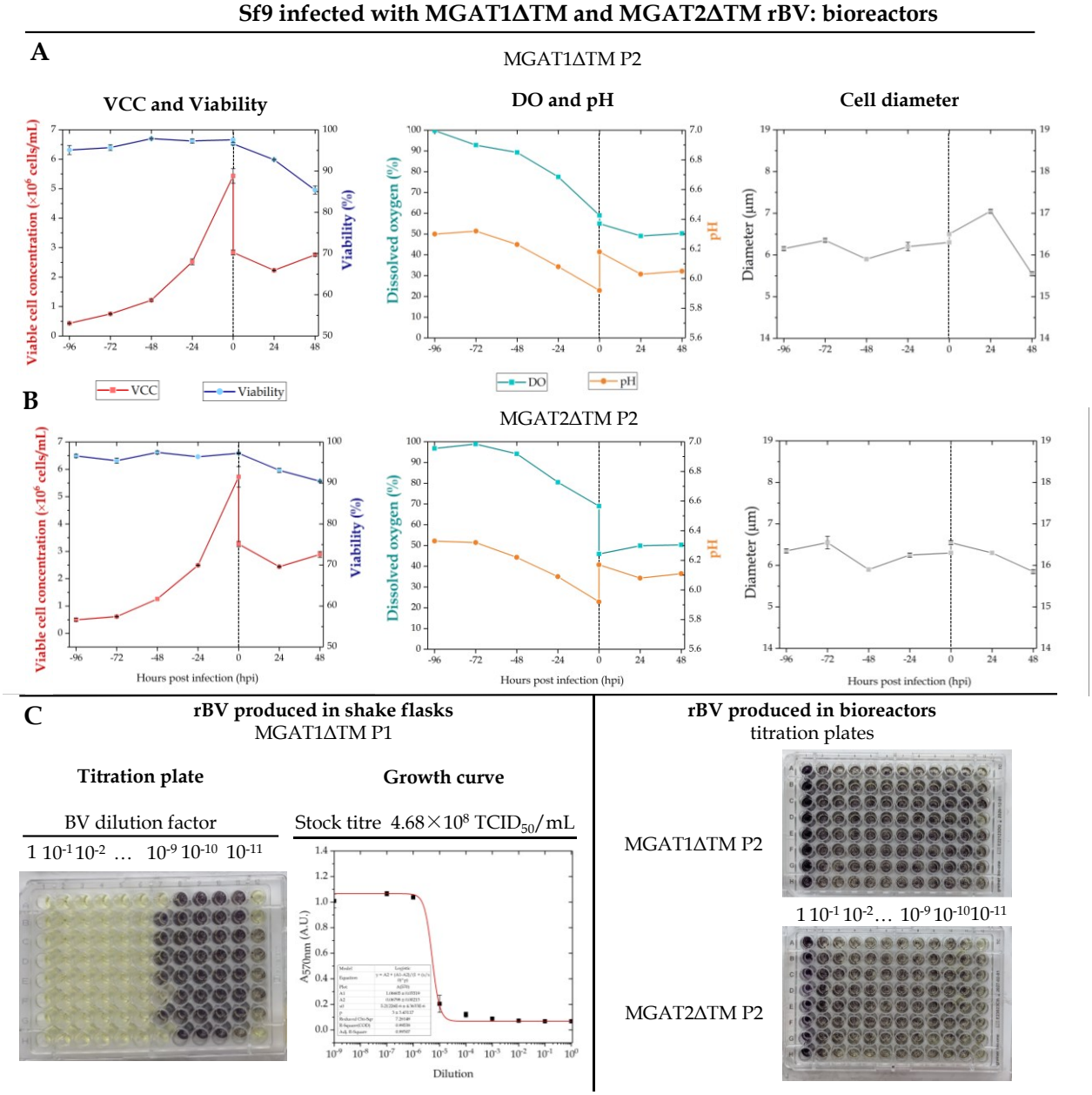

Figure 7. Key results from the production of MGAT1ΔTM and MGAT2ΔTM rBV P2 in bioreactors. **A) Main parameter dynamics during production process:** VCC (red) and viability (blue), DO (cyan) and pH (orange), and cell diameter (grey). Growth phase is represented in the -96 to 0 hpi period; infection phase is depicted within the 0-48 hpi; vertical marker separates the growth and infection time periods in the graphs. VCC, viability, and cell diameter datapoints represent mean values averaged from 2 replicates; error bars show standard deviation. For some datapoints, error bars are smaller than shown symbols. **B) Comparison of rBV stocks titration results:** reference P1 stock titration result produced in small-scale is visually compared to the titration plates of large-scale produced rBV P2 stocks for MGAT1ΔTM and MGAT2ΔTM. Reference is shown using MGAT1ΔTM rBV P1 plate and its corresponding VCC curve (red line), as well as stock titre calculated on the basis of the curve parameters. Each datapoint represents mean absorbance value measured at 570 nm, obtained from 8 biological replicates; error bars show standard deviation per each

datapoint. For some datapoints, error bars are smaller than shown symbols. In all titration plates shown, identical baculovirus dilution factors were tested (10^{0}-10^{-11}).

3.2 Production of monoclonal antibody Rituximab

3.2.1 Determination of optimal conditions for Rituximab expression

Per each of the transfer vector designs (dV encoding both LC and HC of Rituximab; LC mV; HC mV), a separate set of recombinant baculovirus stocks was established. During P0 production, no assessment of the infected cell culture dynamics or produced rBV was performed. Directly amplified from P0, P1 stocks were characterized by infectious rBV titres within 10^{6}–10^{7} range per each transfer vector construct (Table 5), insufficient for expression experiments in insect cells with high infectious doses (MOI). To achieve higher rBV titres, secondary amplification of P1 stocks was performed for all three constructs. P2 stocks for LC and HC mV constructs achieved rBV infectious titre within 10^{8} range, that being a 10^{1}–10^{2} increase from the P1 values (Table 5). rBV titre for dV, however, only improved tenfold for P1, rising from 10^{6} to 10^{7}. Another amplification round for P2 rBV stock of dV construct was not performed to avoid accumulation of undesirable mutations in rBV affecting recombinant protein expression (OET Ltd. 2016).

TABLE 5. Infectious titres of rBV P1 and P2 stocks for each of the transfer vector construct design for Rituximab production.

Transfer vector construct	Promoter	rBV titre ($TCID_{50}$/ml)	
		P1	P2
LC-HC dual vector	LC: *p10*; HC: *polh*	2.75×10^{6}	1.40×10^{7}
LC monopromoter	*polh*	4.19×10^{6}	3.75×10^{8}
HC monopromoter	*polh*	2.37×10^{7}	3.03×10^{8}

Using produced baculovirus stocks, both transfer vector design approaches (dV and mV) were tested in expression experiments. First, HighFive™ cells were infected with dV rBV P2 stock at MOI of 1 and 5 IP/cell, most common infectious doses utilized for antibody expression in baculovirus-insect cell systems (Cérutti & Golay 2012). Volume of P2 stock that was required to achieve MOI of 5 constituted half of the total working volume of the experiment variant, hence the cell suspension was supplemented with 5% of chemically defined feeding supplement, intended to compensate for the excessive dilution of the culture medium. In the experiment, cell dynamics during infection corresponded well to the typical baculovirus infection progression observed in enzyme production (data not shown). Both variants infected with MOI 1 and MOI 5 IP/cell, as well as uninfected control, exhibited substantial increase of VCC one day after infection (24 hpi), as concentrations doubled (for MOI 1 variant) or nearly tripled (for MOI 5 and control) (Figure 8A). Viability only slightly increased at 24 hpi, while cell diameter, on the opposite,

lowered insignificantly in all investigated conditions. The following day (48 hpi) only moderate increase in VCC was detected for all three variants, and viability started to drop to around 90% in all conditions, including control. Cell diameter at 48 hpi recovered to the initial values of around 20.4 µm for both MOI 1 and control conditions, while cells in MOI 5 variant continued to shrink, settling at 19.6 µm. MOI 5 variant outperformed MOI 1 variant in all parameters for cell dynamics during infection, demonstrating better cell condition associated with presence of the feeding supplement. Despite that, cell viability of all investigated variants displayed signs of stagnation at 48 hpi. To prevent potential cell lysis during progressing viability decline, and subsequent proteolytic degradation of expressed Rituximab, experiment was terminated at that point.

Next, assessment of Rituximab expression using mV constructs was carried out by infecting HighFive™ cells with MOI 1, 5, and 10 IP/cell of P2 rBV stocks for LC and HC in several ratios (Figure 8B), with the intent to determine a ratio of antibody chains yielding the best assembly of full-length heterodimer. As per literature recommendations for mammalian cells, excess of LC was maintained in the investigated variants (Zhang et al. 2022). During infection, most of the tested conditions displayed trends in VCC, viability, and cell diameter similar to those observed in dV experiment. Notable exceptions include variant 9, which contained the highest amount of baculovirus, and thus exhibited the most moderate VCC increase at 24 and 48 hpi, and the most prominent viability decline within the same period. As already seen with dV construct, majority of variants, as well as control, experienced a considerable viability drop at 48 hpi; unlike dV test, most conditions reached viability in the 80–90% range at 48 hpi, while two conditions with high baculoviral doses, 6 and 9, dropped below the 80% threshold. Due to the cell dynamics being similar to the dV experiment, mV construct expression test was terminated at 48 hpi. Within studied 48 h, cell diameter for all conditions fluctuated within a ± 1 µm range. Routinely observed stability of the cell diameter values throughout the course of infection was associated with lack of accumulated antibody product within the cells, and its secretion into culture medium.

Analysis of both expression tests with SDS-PAGE yielded no clear indication of presence or absence of Rituximab (Figure 8). Concentrated extracellular samples collected throughout the infection duration showed identical protein band composition in uninfected controls and infected samples. Intensity and thickness of the bands in all samples within the molecular weight regions of interest (150+ kDa for assembled mAb, 55 kDa for HC, 25 kDa for LC) varied from sample to sample without a concise trend, and thus no confident conclusion could be drawn from the conducted SDS-PAGE assessment. Intracellular fractions of all infected variants were also studied for presence of mAb-attributed bands, and none were identified (data not shown).

A more in-depth investigation was performed on the supernatant harvest of the samples infected at highest MOI conditions per each construct (dV: condition 2; mV: condition 2, 3, 5 (MOI 5 IP/cell) and 3, 6, 9 (MOI 10 IP/cell)). To increase the chances of identifying protein bands corresponding to Rituximab,

for each selected sample, 10 ml of supernatant harvested at 48 hpi were concentrated 10 times and studied through SDS-PAGE and Western blot. Protein band composition obtained from SDS-PAGE was not conclusive, similarly to earlier results with less concentrated samples (data not shown). Western blot revealed that, in all studied conditions, assembly of full-length antibody was minimal, with predominantly free chains being expressed (Figure 9). Among two tested transfer vector constructs, dual vector design has shown outstanding advantage in producing Rituximab over monopromoter counterpart. Cells infected with MOI 5 of dV formed two protein species that could be considered as versions of a full-length mAb, with one band observed in the MW region of 180+ kDa, and another aligned at 180 kDa marker band. Both bands were within the reference MW region, established from an analytical-grade reference Rituximab molecule produced in mammalian cells.

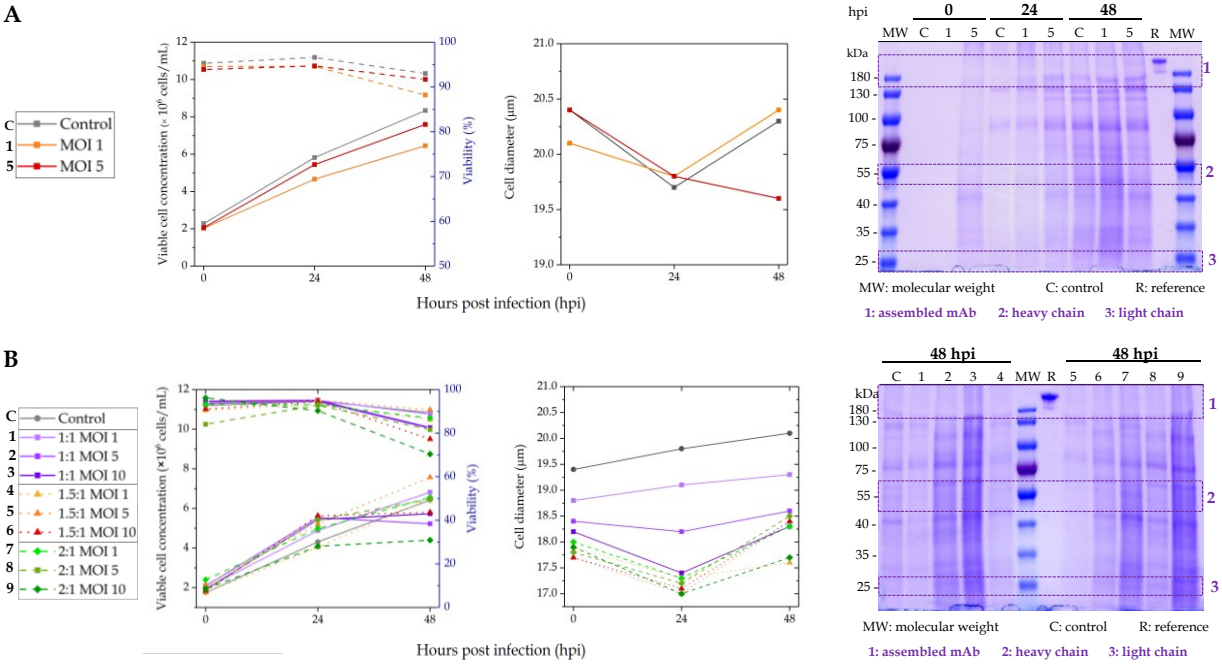

Figure 8. Cell dynamics and SDS-PAGE assessment of Rituximab expression tests using two transfer vector construct designs**. A) Expression using dV construct:** each variant (uninfected control C; infection with MOI 1IP/cell (1); infection with MOI 5 IP/cell (5)) are represented by the same colour: grey for C, orange for 1, red for 5. VCC trends (left Y-axis, in black) are shown in normal lines, viability data (right Y-axis, in blue) is plotted with dashed lines**.** SDS-PAGE gel visualizes protein content dynamics following infection progression for all tested variants (0-48 hpi). **B) Expression using mV constructs:** ten tested variants are highlighted in assigned colours: uninfected control (C) is in grey; variants with different LC:HC ratios are depicted through groups with similar shading and line styles. Purple-shaded normal lines represent 1:1 ratio group with intensifying MOI dose reflected in colour; dotted orange-red lines are for 1.5:1 ratio group; dashed green lines depict 2:1 ratio group. SDS-PAGE gel shows protein content obtained from the last day of infection (48 hpi). For both A and B sections, three areas of interest are highlighted in SDS-PAGE gels with purple

dashed figures. Each well represents protein content from 500 µl supernatant concentrated 10 times, prepared in non-reducing conditions. Reference well contained 0.5 µg of denatured antibody.

Separation between the two bands likely occurred due to several reasons, namely: structural differences directly affecting MW, variations in PTMs, including glycosylation, or denaturing conditions used for sample preparation. As for the mV-derived samples, none of the chain ratios, as well as neither infectious doses of MOI 5 and MOI 10, resulted in assembly of Rituximab heterodimer. Only faint bands in the regions of heavy and light chains were observed. Intensities of the observed chain bands in mV samples differed slightly between three tested LC:HC ratios, however, the variations were not considered significant enough to confidently choose a better performing chain ratio. Notably, in all samples obtained from insect cells, heavy chain and light chain protein bands migrated to a lower MW region than those in reference Rituximab molecule. Since the MW difference was roughly within 5 kDa, this phenomenon was attributed to varying PTMs. Based on the overall obtained data, a preference for use in Rituximab expression was given to dV construct stocks. In addition, a strategy to improve Rituximab assembly needed to be developed.

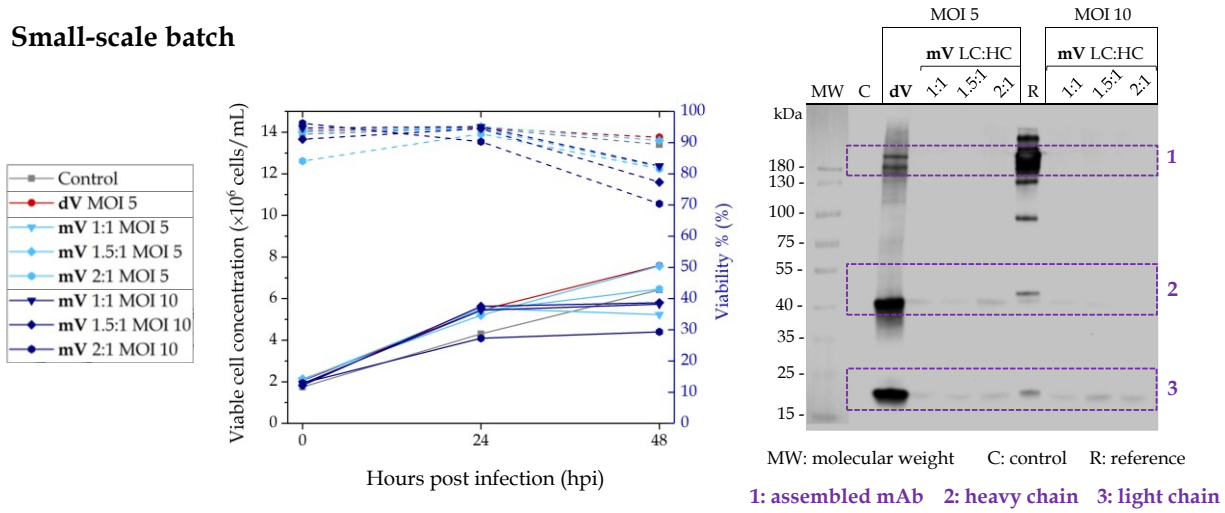

Figure 9. Key results from the small-scale batch expression tests using dV and mV construct stocks. Data for variants infected with the highest MOI is depicted (MOI 5 IP/cell for dV test, MOI 10 IP/cell for mV test). For comparison of construct design performance, MOI 5 results from mV test are included. Cell dynamics graph shows the dynamics of VCC (left Y-axis, in black) and viability (right Y-axis, in blue) during infection (48 hpi for both tests). VCC data is represented through normal lines; for viability, dashed lines are used. Uninfected control (from dV test) is in grey line, dV variant is in red, and mV variants are grouped in light blue colour (MOI 5 conditions with different LC:HC ratios) and dark blue (MOI 10 IP/cell) colour. In Western blot, three areas of interest are highlighted with purple dashed figures. Protein content in each well was derived from sample of 10 ml supernatant concentrated 10 times. All depicted samples were run in non-reducing conditions. Reference well contained 0.5 µg of

denatured antibody. Contrast and saturation of the original Western blot image were modified to better visualize the bands.

To aid assembly of full-length Rituximab, a combination of several approaches was chosen: change of cell cultivation method from batch mode to fed-batch, and supplementation of additives capable of enhancing antibody structure. In fed-batch mode, regular addition of nutrient supplements to infected cell culture was meant to improve cell condition during infection, thus supporting protein synthesis and processing, and prolong duration of infection timeline, resulting in larger quantities of properly assembled mAb. To further assist association of individual chains into the heterodimer, addition of Cysteine and Trehalose was tested. Cysteine was used to modulate redox potential of the infected cell culture towards oxidizing conditions (Komuczki et al. 2022) in order to improve the quality of interchain disulphide bonds, while Trehalose, regarded in the literature as "chemical chaperone" (Leibly et al. 2012), was tested as a support to the innate HighFive™ chaperone proteins responsible for the assembly of recombinant proteins. Using the only available chemically defined feeding supplement, HEK FS, two feeding strategies were designed: one based on the manufacturer's guidelines, with daily feedings, and an alternative, where feeds were introduced as bolus once every two days, the latter being a common strategy employed in mammalian cell culture fed-batch (Xu et al. 2023). Effects of Cysteine and Trehalose were studied in both strategies: 130 µM of L-Cysteine were added at 72 hpi to respective variants, and 75 mM Trehalose was supplemented to the cell culture medium at infection timepoint in chosen variants. Concentration of L-Cysteine was proposed by research group colleagues with prior experience in additive supplementation, and Trehalose dose was taken half of that reported in the literature (Onitsuka et al. 2014). Unfortunately, due to consistently low titres of dV rBV stocks, this construct could not be used in the fed-batch test, as stock volume was not enough even for a small-scale expression. Instead, low-performing mV stocks had to be utilized with LC:HC ratio 1:1. In order to maximize the chances of obtaining assembled antibody from this construct, baculovirus dose at MOI of 20 IP/cell was applied.

As anticipated, VCC and viability dynamics in fed-batch mode displayed an overall more desirable trend than that seen in batch test experiments (Figure 10). Duration of baculovirus infection in both strategies was prolonged to 6 days (144 hpi) compared to 2 days (48 hpi) in batch mode without exceeding viability threshold. Peak VCC values achieved in both feeding strategies (on average, 8×10^6 cells/ml in strategy 1; 10×10^6 cells/ml in strategy 2) were about two times higher than those exhibited in batch mode (on average, 4.5×10^6 cells/ml). Similarly to batch experiments, cell diameter did not experience clear increase throughout the infection timeline (data not shown). Due to rapid growth of infected cells in all variants, temperature shift was performed on day 3 (72 hpi) to stabilize VCC and viability. At the same timepoint, L-Glutamine was added to all variants to sustain cell growth. Stabilization of cell dynamics trends was achieved successfully for most of the experiment variants, except for conditions supplemented with Trehalose, which experienced noticeable fluctuations in VCC

and viability in the later stages of infection. Addition of Cysteine did not affect any observed parameters. After harvest, supernatant samples were prepared for SDS-PAGE and Western blot in the same manner as described for in-depth assessment of batch experiments. SDS-PAGE was again not informative (data not shown), while Western blot showed that improvement in full-length Rituximab assembly was not achieved under any investigated conditions. Just as observed in batch test, primarily free chains were abundant in cell supernatants. In fed-batch experiment, their intensity was higher, which could be attributed to both higher MOI condition and nutrient supplementation. An improvement from batch experiments was appearance of protein bands in the MW region corresponding to the complete mAb. Those manifested only in samples cultivated with feeding strategy 1. Among conditions tested within strategy 1, no significant difference was observed between the bands in the 150+ kDa MW region. While intensity of the full-length mAb bands in flasks supplemented with Cysteine and Trehalose was more prominent than that of the normally fed flask, the difference was not remarkable enough for these additives to be considered for future applications. Thus, feeding strategy 1 without additives was chosen as the optimal expression setup for production of Rituximab in HighFive™ cells.

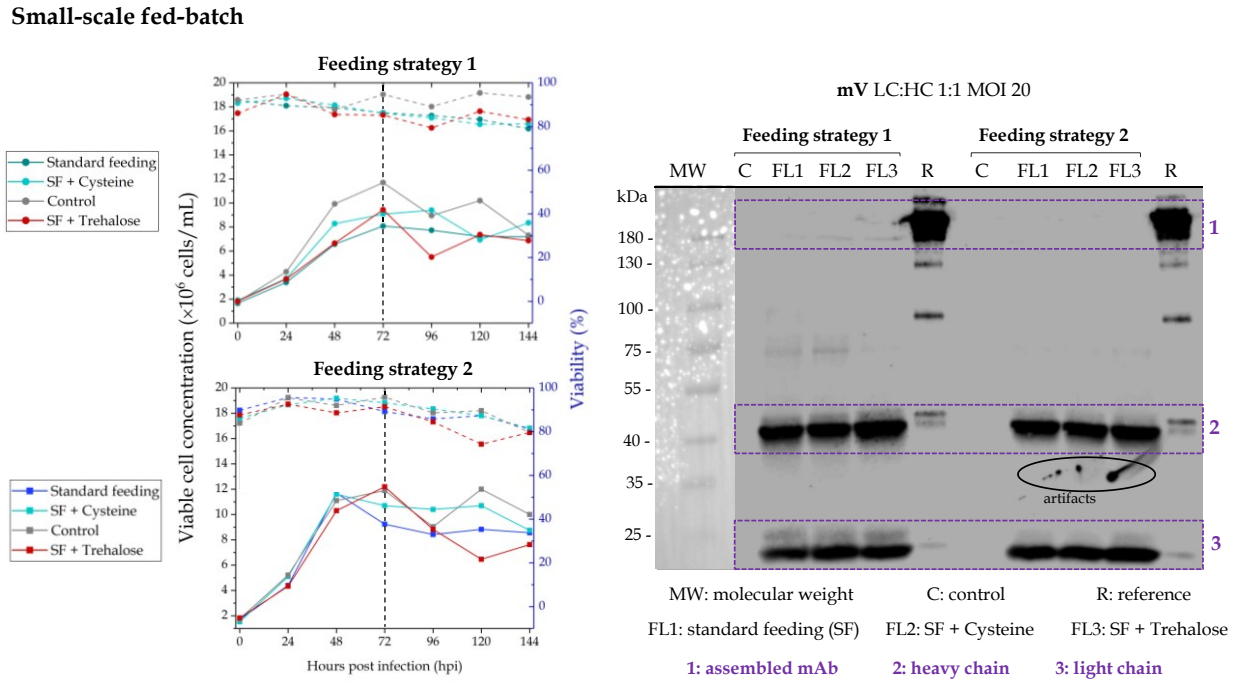

Figure 10. Key results from the small-scale fed-batch expression tests using infectious dose of MOI 20 IP/cell of mV construct stocks. Cell dynamics for two tested feeding strategies shows VCC (left Y-axis, in black) and viability data (right Y-axis, in blue) throughout infection timeline. Conditions that contain Cysteine are highlighted in cyan colour; presence of Trehalose is shown through red colour. Uninfected controls are grey. VCC data is depicted through normal lines, viability data is in dashed lines. Vertical dashed lines in cell graphs indicate temperature shift from 28 to 20 °C, and simultaneous supplementation with L-Glutamine. In Western blot, three areas of interest are highlighted in purple

dashed figures. Protein content in each well was derived from a sample of 10 ml supernatant concentrated 10 times. All depicted samples were run in non-reducing conditions. Reference wells contained 0.5 µg of denatured antibody. Contrast and saturation of the original Western blot image were modified to better visualize the bands.

Antibody and its heavy chain fragments from all conditions tested in both batch and fed-batch experiments were pooled and purified using protein A/G affinity chromatography, producing eluate containing only 7.7 µg ± 0.4 µg of Rituximab variants. This amount was not sufficient for planned IVGE tests, and therefore, one last expression experiment was performed with a focus on producing maximal amount of Rituximab material. For that purpose, large-scale setup with bioreactors was chosen. In the same run, a final test of modulating cultivation conditions for improvement of disulphide bond quality was planned. Using controlled environment of the bioreactors, dissolved oxygen concentration threshold was set at 50% with the aim of providing optimal oxidative conditions for disulphide bond establishment, and subsequent free chain association into a desired antibody format.

3.2.2 Large-scale production of Rituximab

The large-scale production attempt was performed in two bioreactors (Figure 11A). For infection, fresh rBV P2 stock of dV construct was amplified from previously established P1 material. Similarly to the value of the first P2 stock, infectious titre of the new small-scale amplified stock constituted 1.16×10^7 $TCID_{50}$/ml. With that titre and obtained volume, only infectious doses of MOI 1 IP/cell for one of the bioreactors (Bioreactor 1), and MOI 0.1 IP/cell for another (Bioreactor 2) could be utilized. During growth phase (-48 to 0 hpi; Figure 11A), VCC increased steadily in the growth bioreactor unit until -24 hpi (in Figure 11A, data for growth period is represented by Bioreactor 2 line), and viability remained well above 90%. At 24 h until infection, sparging was accidentally shifted from macrosparger to microsparger, intended for post-infection culturing, before time of infection. Because of higher shear stress load from premature microsparger activation, the cells sustained extensive damage from shear stress. As a result, over the next 24 h, rapid drop of cell viability from 90+% to 40% occurred, and VCC stopped at around 2×10^6 cells/ml. While the sparging rate was decreased tenfold at the time of infection, cellular viability remained affected throughout the entire duration of the infection in both bioreactors: the values continued to slowly decrease despite daily supplementation of nutrient-rich feeding solution. VCC values displayed a more positive trend, with slight increase per each day of cultivation until 120 hpi, when concentrations dropped in both units. The highest VCC achieved in both units was around 2.5×10^6 cells/ml, nearly 4 times lower than the highest VCC values achieved with the same feeding strategy in small-scale fed-batch. Bioreactor 2, infected with lower virus dose, reached higher cell densities throughout infection timeline. Due to moderate growth trend, no temperature shift or L-Glutamine supplementation

were implemented in the large-scale process. DO concentrations remained above 50% threshold throughout the entire infection period (data not shown).

Harvested supernatant for each unit was individually processed in protein G affinity chromatography, where two expected structural variants of Rituximab (assembled heterodimer LC2HC2 and HC) were set to elute in four steps (Figure 11B). Each step contained a specific concentration of low-pH elution buffer (25-50-75-100%), aimed to separate the variants based on their affinity to the column matrix. As both bioreactors were infected with low doses of rBV, resulting absorption peaks detected at 280 nm were expected to be very low and hard to detect. To enhance product detection in eluate through peptide bond tracing, UV absorbance at 220 nm was monitored. Unlike expected, three absorption peaks (220 nm data) emerged in the eluate during two chromatographic runs. Concentrated fractions corresponding to each peak were first studied in SDS-PAGE to identify their protein content, but due to low informativity of the result (data not shown), were pooled together. The pool was assessed in SDS-PAGE and Western blot to obtain an overview of the protein composition of the final product (Figure 11C). SDS-PAGE did not produce any comprehensive result, but in Western blot, three structural entities of Rituximab were seen: single band within the MW region of a fully assembled mAb, three bands likely corresponding to heavy chain, and a single band in the light chain region. Presence of light chain in non-reducing conditions was untypical, since protein G does not bind this species, suggesting that free light chain possibly originated due to full-length mAb degradation during storage or handling. Based on the band intensity of all three species, any effect of DO concentration on mAb assembly was not observed, as the intensities of bands of interest were the same as in previous expression experiments. Unlike earlier, heavy chain manifested as three individual bands, with two of them being notably lower in molecular weight than the band from the reference Rituximab. The same misalignment of the insect cell-derived Rituximab bands happened for full-length mAb, which was below the 180 kDa molecular ladder marker and the monomer band from reference molecule. Observed behaviour could be linked to the shear-stressed condition of the infected cells, resulting in additional disruptions of recombinant protein processing. Nonetheless, three mAb-attributed protein species could still be safely identified in the established stock with total antibody content accounting to 351.1 µg ± 7.8 µg. Altogether, material obtained for *in vitro* glycoengineering constituted of a minor portion of full-length Rituximab, and a large share of free heavy chain.

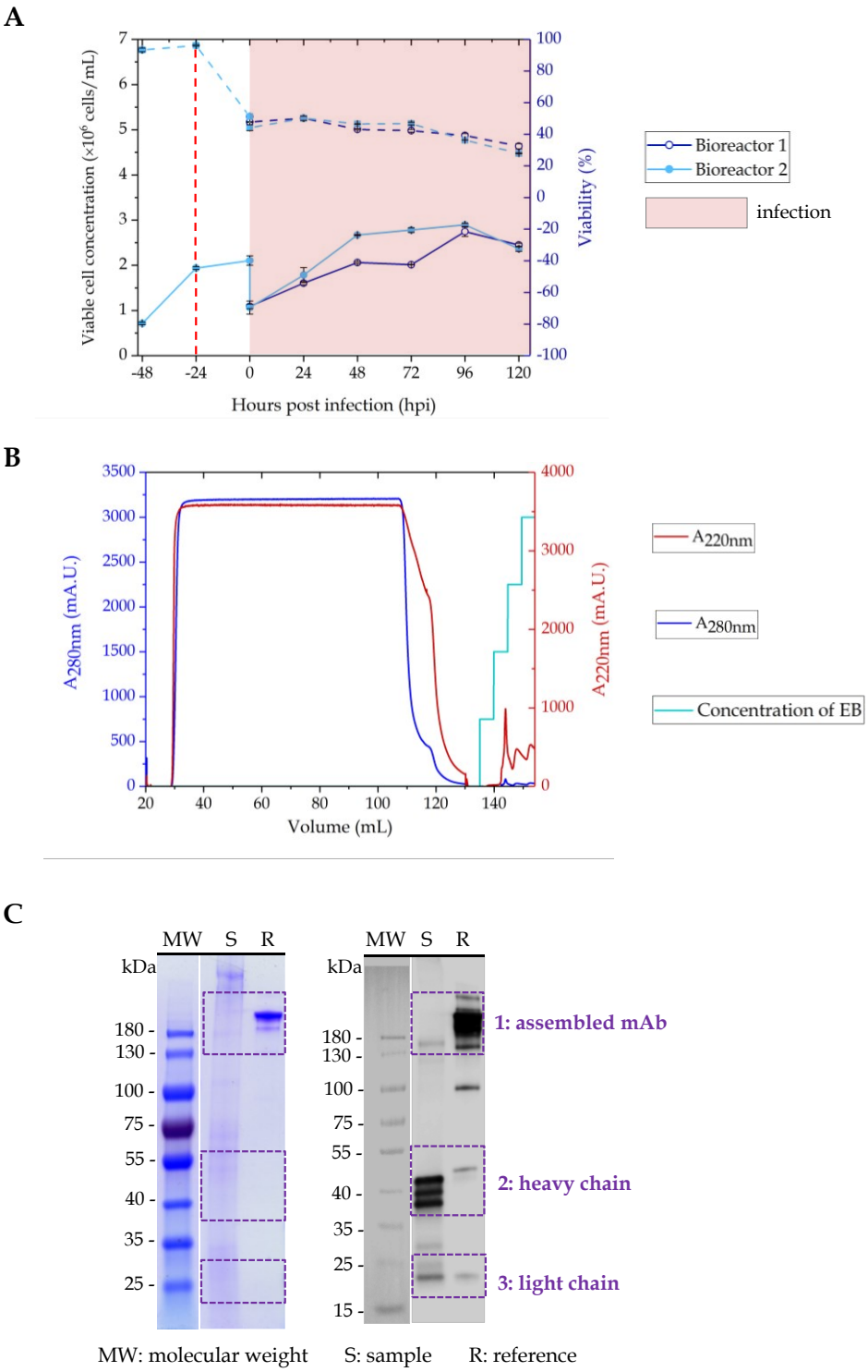

Figure 11. Results from three steps of production of Rituximab in large scale. **A) Expression** section depicts cell dynamics during growth and infection periods in two bioreactors. Data for bioreactor 1 (infected with MOI 1 IP/cell) is in dark blue; data for bioreactor 2 (infected with MOI 0.1 IP/cell) is in light blue. Dashed red line indicates the timepoint of sparging mistake. Red shading of in the graph corresponds to infection timeline. VCC data (left Y-axis, in black) represents averaged values obtained from 2 biological replicates; each datapoint has error bars showing standard deviation. For some datapoints, error bars are smaller

than the symbols used. The same applies to viability data (right Y-axis, in blue); trends for each condition are shown in dashed lines. **B) Purification** section shows protein G affinity chromatography procedure. UV absorbance was tracked at 280 nm (blue line; left Y-axis, in blue) and 220 nm (red line; right Y-axis, in red). Elution process (starting at 135 ml) contained four steps highlighted through cyan colour, which represents concentration of elution buffer (25-50-75-100%). **C) Assessment** section shows results for SDS-PAGE and Western blot of concentrated eluate pool collected after purification (S), and reference Rituximab (R; 0.5 µg/well). All depicted samples were run in non-reducing conditions.

3.3 IVGE of Rituximab

N-glycan modification on Rituximab material obtained from HighFive™ cells was performed in two steps. First, starting *N*-glycoprofile of the antibody material, derived from large-scale production, was characterized using xCGE-LIF (data in grey in Figure 12). Carbohydrates released from nonmodified Rituximab produced glycoprint containing structures of three *N*-glycan classes: paucimannose, high-mannose, and complex (Figure 12). Despite classification variety, *N*-glycan composition was characterized by relative homogeneity, with only three peaks with intensity values above 10% of total peak height (TPH), a threshold determining significance of the data. Dominant species in the glycoprofile were represented by a main peak with intensity of 50% TPH, emerging at 220.8 MTU''. Software database could not identify corresponding glycan structure, but it was presumed to be core α1,3/6-difucosylated Man3F(α1,3)F, *N*-glycan epitope commonly found on insect cell proteins (Stanton et al. 2017). Two other significant peaks were found at 254.7 MTU'' and 358 MTU''. The 254.7 MTU'' peak was annotated as a complex monosialylated structure S1(α2,3)G2F, while glycoform behind the smaller peak at 358 MTU'' was not recognized. Other minor annotated peaks were attributed to Man3F structure (206.2 MTU''), and to high-mannose Man5 *N*-glycan, or/and complex glycoform G0F-Gn (247.6 MTU''). Altogether, two carbohydrate structures desirable for the planned IVGE procedure were present in the *N*-glycosylation pattern of Rituximab species – Man3F and Man3F(α1,3)F, with the target Man3F(α1,3)F species being dominant in the non-modified antibody material.

After establishing the starting glycoprofile of HighFive™ Rituximab mixture, two separate IVGE experiments were done on large-scale fed-batch product. In the first experiment, planned *in vitro* glycoengineering using recombinant glycosyltransferases MGAT1ΔTM, MGAT2ΔTM, and GalTΔTM, expressed in *E.coli*, was done. In the second, the same glycosyltransferases expressed in HighFive™ were applied. Due to extremely low amounts of insect cell-derived MGAT1ΔTM and MGAT2ΔTM, standard incubation time for reactions with these enzymes was doubled, and content of MGAT1ΔTM stock was supplemented with eluate from large-scale purification optimization experiment. Eventually, MGAT1ΔTM concentration in insect cell experiment was 18 times lower than the target (employed with the *E.coli* enzymes), while concentration of MGAT2ΔTM was 3 times lower.

N-glycoprofile assessment of the endpoint mAb products obtained after completion of both experiments revealed that the tested IVGE setup successfully achieved desired conversion (Figure 12). Indeed, in either experiment, intensity of the target Man3F(α1,3)F glycan peak, presumed in the starting fingerprint (grey colour), decreased drastically. In the *E.coli* enzyme experiment (blue line; Figure 12A), only a trace of the peak in the same position was left, whereas in case of the HighFive™ (pink line; Figure 12B) enzyme run, no peak was found in the position of the original, indicating 100% conversion rate. In both experiments, prominent new peaks emerged at 363.4 (HighFive™)/363.6 (*E.coli*) MTU''. Similarly to the starting peaks, glycan structure for the new peaks was not recognized by the software. However, presence of an adjacent minor peak at 359.4 MTU'', which was annotated by the software as G2F, indicated that the peak of interest represented a rather similar in size (mass-to-charge ratio), charge, and shape (hydrodynamic volume) glycoform. Therefore, the newly emerged prominent peak in both glycoengineered samples was attributed to core α1,3/6-difucosylated G2F(α1,3)F. In the same manner as for the major peaks bearing core α1,3-linked fucose, minor monofucosylated G2F peaks appeared in the glycoprofiles of both IVGE experiments, resulting from full conversion of its original substrate Man3F: no peaks remained in the position corresponding to Man3F after IVGE with both *E.coli* and HighFive™ enzymes.

Intriguingly, peaks corresponding to Man5 and/or G0F-Gn (247.6 MTU''), as well as S1(α2,3)G2F (254.7 MTU''), seen in the data for original Rituximab before IVGE, disappeared completely from the fingerprints of the glycoengineered mAb. All three structures, though not considered as typical substrates for employed glycan modification, could have been elongated by the activity of the enzymes utilized in the tested IVGE approach. As for the first peak, elongation of Man5 would start from terminal mannose in α1,3 position, catalysed by MGAT1ΔTM; MGAT2ΔTM could add GlcNAc residue to the α1,6 mannose of G0F-Gn, if this glycoform was present in the sample, allowing subsequent galactosylation by GalTΔTM. Supposed extension of S1(α2,3)G2F would occur in α1,3 antenna through sequential activity of all three glycosyltransferases, with terminal galactose as a starting point. Thus, certain unrecognized peaks in the demonstrated fingerprints could represent fully or partially modified glycan structures. Alternatively, new peaks representing them could appear in the electropherogram beyond studied range (from 400 MTU'' onwards).

To further evaluate resulting *N*-glycoprofile of *in vitro* glycoengineered Rituximab material, it was compared with the glycoprofile of reference Rituximab, commercial clinical-grade mAb bearing nonmodified mammalian (CHO) cell glycans (Figure 13). For this purpose, fingerprint from the IVGE experiment with HighFive™-produced glycosyltransferases was used. When compared, glycan profile of glycoengineered mAb demonstrated higher homogeneity than one from the commercial counterpart. Only a single peak with the intensity of above 10% TPH appeared in the electropherogram of modified Rituximab, while, in case of reference, four significant peaks were observed. The

four peaks indicated large presence of core α1,6-fucosylated agalactosylated *N*-glycans (G0F), as well as glycans with a single galactose moiety in either α1,6 arm (G1F(6)) or α1,3 arm (G1F(3)); agalactosylated and monogalactosylated in α1,6 arm glycoforms were the most abundant on the reference protein, as the intensity of each respective peak accounted for around 40% TPH. The least abundant identified carbohydrate for the reference Rituximab was terminally digalactosylated glycan with α1,6 core fucose (G2F), accounting to about 13% of TPH. In contrast, single major peak in the glycoengineered Rituximab *N*-glycan fingerprint indicated dominance of unconfirmed but presumed digalactosylated and core α1,3/6-difucosylated structure (G2F(α1,3)F) in the *N*-glycoprofile, as its intensity constituted more than 75% TPH. The only annotated minor nonsignificant peak corresponded to G2F structure, potentially less common on the glycoengineered sample (~5% TPH) than on the reference mAb (~13% TPH). Overall, IVGE approach produced glycosylation profile on insect cell-derived therapeutic mAb Rituximab that was superior in homogeneity and galactosylation level to the mammalian cell-derived commercial equivalent.

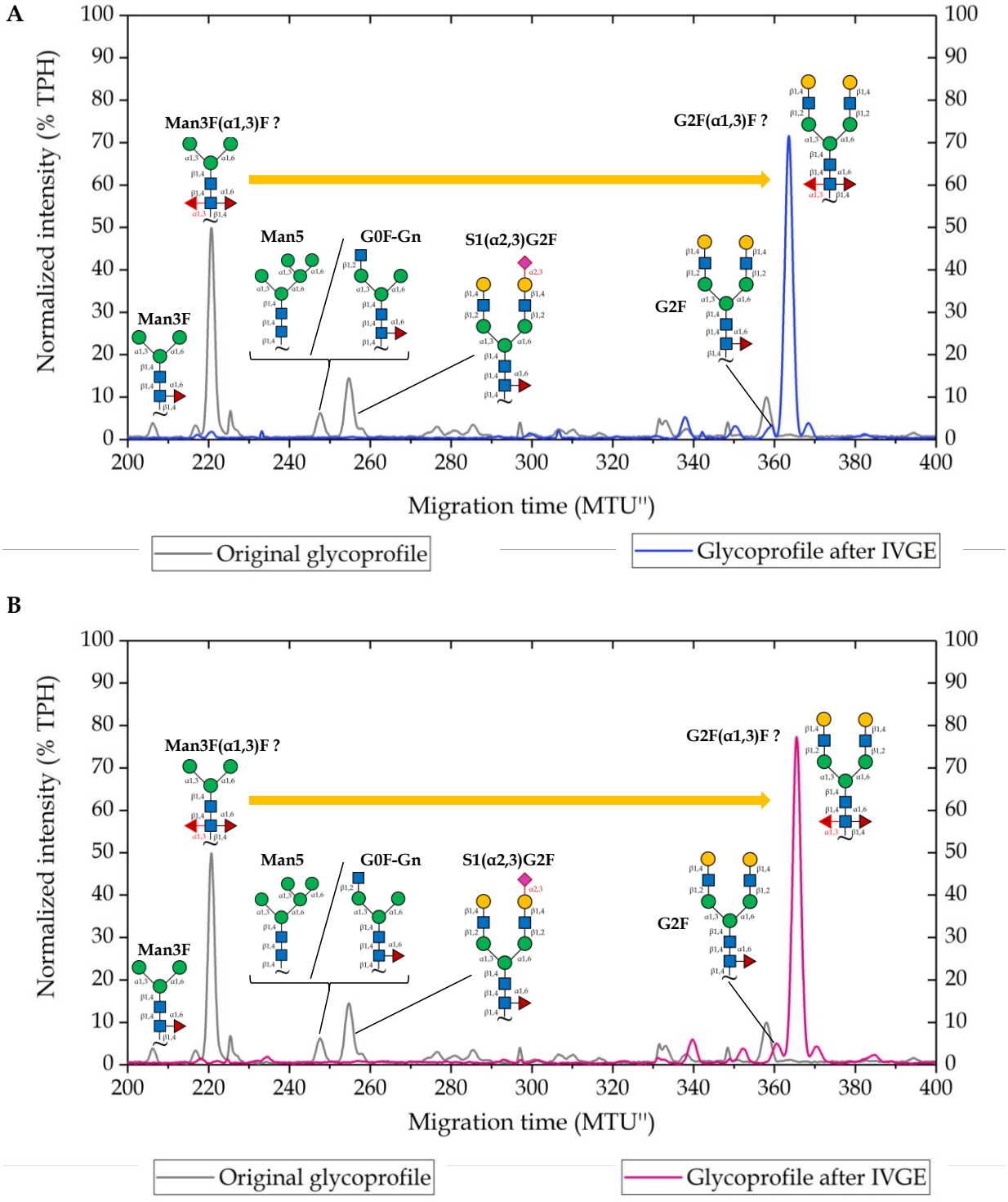

Figure 12. xCGE-LIF *N*-glycan fingerprints of non-*in vitro* glycoengineered (original) Rituximab from insect cells and *in vitro* glycoengineered (after IVGE) using 3 recombinant glycosyltransferases expressed in two hosts. Original Rituximab *N*-glycoprofile (depicted in grey) was derived from large-scale production sample. *N*-glycosylation pattern obtained after IVGE using glycosyltransferases **expressed in *E.coli* (A)** is shown in blue, and after IVGE using glycosyltransferases **expressed in HighFive™ (B)** in pink. Endpoint *N*-glycoprofile after 3 glycoengineering reactions is shown per each IVGE test. Conversion of

the starting glycoforms is shown with orange arrows. Unnatural to humans glycosidic linkages are highlighted in red colour on *N*-glycan structures.

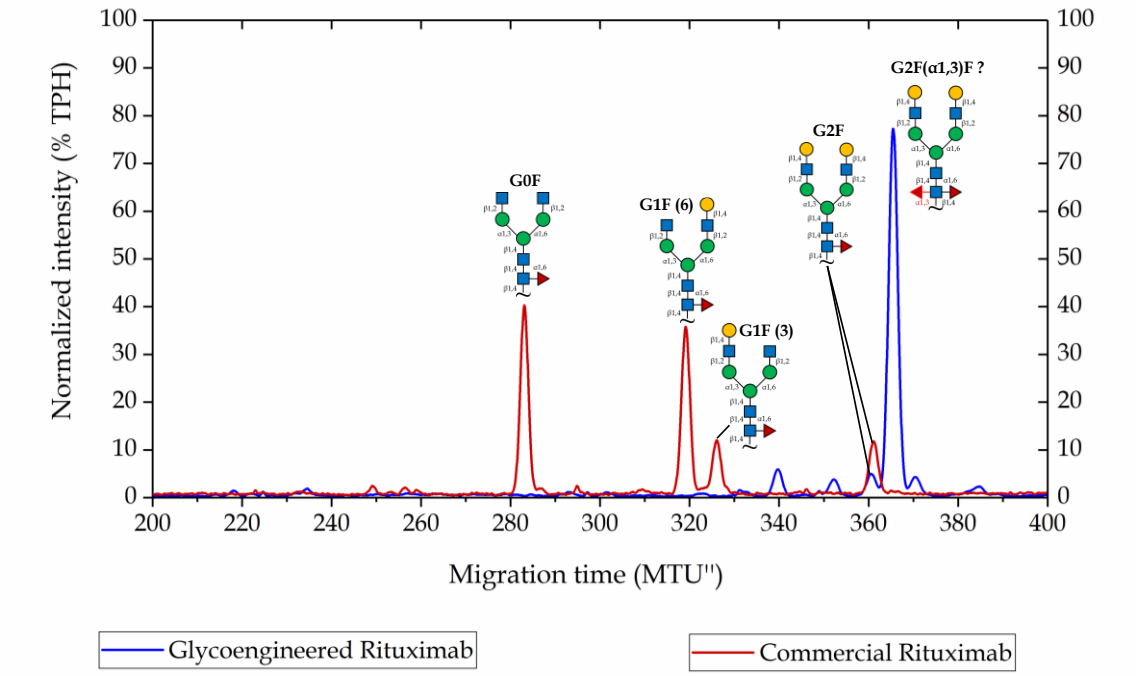

Figure 13. xCGE-LIF *N*-glycan fingerprints of *in vitro* glycoengineered Rituximab from insect cells (blue) obtained with HighFive™-derived enzymes and non-glycoengineered reference commercial Rituximab from mammalian cells (red).

4 DISCUSSION

Monoclonal immunoglobulin G antibodies, a dominant class of therapeutic proteins, fail to achieve their maximum immune-modulating potential due to inherent macro- and microheterogeneity of glycosylation pattern, dictated by mammalian expression hosts routinely utilized for commercial mAb production. Despite a variety of glycan modification methods having been introduced in the last decades, only a few glycoengineering strategies that overcome oligosaccharide microheterogeneity exist. Thus, developing an effective approach that enhances *N*-glycan galactosylation, sialylation, and core afucosylation levels, essential for increasing the magnitude of target immune response, remains a priory in the field of industrial biotherapeutics. In this work, a novel chemoenzymatic *in vitro* glycoengineering method for therapeutic IgGs was successfully implemented using Lepidopteran insect cells as heterologous expression hosts for both the enzymes and a model antibody Rituximab, chimeric mouse-human IgG_1. xCGE-LIF-assessed *N*-glycoprofile of the Rituximab material, obtained from benchtop bioreactor-assisted fed-batch expression in

baculovirus-infected HighFive™ cells, was expectedly dominated by paucimannose *N*-glycans, the substrates for the tested IVGE strategy, with lesser presence of high-mannose and complex bi-antennary glycoforms. By utilizing three-reaction cascade involving recombinant human glycosyltransferases MGAT1ΔTM, MGAT2ΔTM, and GalTΔTM, simple paucimannose *N*-glycans on species of Rituximab were sequentially converted into complex-type bi-antennary structures with terminal galactosylation, highly desired on therapeutic mAbs for eliciting immune response-modulating effector functions complement dependent cytotoxicity and antibody dependent cellular cytotoxicity. Resulting endpoint *N*-glycan fingerprints proved effectiveness of the IVGE strategy on supposedly Man3F(α1,3)F, dominant HighFive™-produced *N*-glycoform, and Man3F, standard paucimannose *N*-linked oligosaccharide, demonstrating full conversion of the starting carbohydrates into desired structures. Furthermore, miscellaneous high-mannose and complex *N*-glycans found on unmodified mAb species underwent conversion during IVGE, likely induced by the enzymatic reactions, and further demonstrated exemplary performance of the glycoengineering strategy. Together with high effectiveness, endpoint *N*-glycan fingerprints of glycoengineered mAb were characterized by noticeable 'cleanliness', as they lacked any notable subproduct peaks of reactions and background intensity noise, common for in-solution chemoenzymatic reactions (Mota et al. 2022). Due to the immobilization of the mAb during IVGE, removal of intermediate by-products of the reactions and the used enzymes allowed to minimize undesirable impurities and cross-reactions (Mota et al. 2022). Successful application of the proposed IVGE method was achieved with glycosyltransferases obtained from the bacterial host (*E.coli*), used in the earlier IVGE studies for expression of the same enzymes (Ruhnau et al. 2021), and eukaryotic host HighFive™, assessed for expression of target glycosyltransferases for the first time in this Master thesis. *N*-glycoprofile resulting from applied *in vitro* glycoengineering using HighFive™-produced enzymes, when compared to the glycosylation pattern of commercial Rituximab, was superior in homogeneity and galactosylation levels, as it was dominated by complex *N*-glycans with digalactosylated antennas, as opposed to primarily agalactosylated and monogalactosylated glycan structures of the non-glycoengineered commercial originator. Full galactosylation of complex *N*-glycan antennas is a crucial precursor towards the universally recognized ''ideal'' *N*-glycan for therapeutic mAbs, S2(α2,6)G2. By achieving a solid advantage in this aspect over the reference mAb, employed IVGE approach exemplified the potential of IgG glycoengineering, and expanded the current set of *in vitro* chemoenzymatic methodologies developed for this type of biotherapeutics. In particular, presented work enriched the state-of-the-art field of mAb IVGE utilizing heterologous hosts for therapeutic antibody expression, in which only a few strategies exist (Mastrangeli et al. 2019). With this approach, homogeneous native insect cell *N*-glycans became the advantageous basis for effective glycan modification, contrary to being regarded as a setback for therapeutic protein

production due to their relative simplicity and lack of diversity (Palomares et al. 2021).

These particular outcomes answered the main research questions set for the current work. However, other objectives of the investigation remain unanswered, and certain aims not achieved. Among them was understanding the suitability of insect cell expression host for glycosyltransferase production, and discovering new host's possible benefits for enzyme performance. As eukaryotes, insect cells offer a wider range of mammalian-like PTMs, compared to the prokaryotic *E.coli* expression host, rendering the recombinant enzymes closer in structure and function to the innate human-derived glycosyltransferases (Moremen et al. 2018). Thus, higher yields and enzymatic activity of the glycosyltransferases recovered from HighFive™ cells than from *E.coli* could potentially be seen in this study. Since *E.coli*-produced glycosyltransferases had to be incorporated in this study due to challenges encountered in the insect cell-based production, a direct comparison for enzyme production between the two hosts can be done. Yields per each enzyme from the two expression hosts indicated significant improvement in values for GalTΔTM, and very slight for MGAT2ΔTM when produced in insect cells; yield of MGAT1ΔTM was superior in *E.coli*. In both hosts, purity of the final product was around 50% per each enzyme. Based solely on these values, insect cell host can be seen advantageous over the *E.coli* one for production purposes, given that planned additional work on enzyme recovery improves MGAT1ΔTM yield, and, desirably, purity of the final product for each of the enzymes. As for the evaluation of the enzymatic activity, production challenges of insect cell-based approach resulted in low amounts of MGAT1ΔTM and MGAT2ΔTM, hence not allowing for a valid comparison with *E.coli* products for glycan conversion activity in IVGE experiments with protein-attached *N*-glycan substrates. Only upon finalizing production strategy for the enzymes, especially MGAT1ΔTM and MGAT2ΔTM, standard conditions proposed for the novel IVGE method can be employed to answer this particular research question. To get there, considerable amount of effort is needed. While a functional insect cell expression protocol for all three glycosyltransferases was developed, enzyme extraction and purification protocols for the first two remained suboptimal by the end of the Master thesis work. Additional tests are required to validate suggested solubilizer-containing extraction and purification buffer formulation, which yielded unclear results in experiments performed on MGAT1ΔTM-containing lysate. For that, production of more cellular material containing enzymes of interest, and a re-test of the solubilizer strategy should be done, including confirmation of the enzyme presence in elution with Western blot. As part of finalization of production strategy in insect cells, large-scale recombinant baculovirus amplification strategy needs to be addressed as well. In the study, bioreactor setup that ensured best possible cell condition during baculovirus infection and amplification achieved just that, as the cells have indeed proliferated until infection, and maintained viability above a set threshold during infection. However, this process resulted in baculovirus stocks with no detected infection potential.

Pinpointing probable reasons behind this phenomenon is complicated, as, apparently, limited number of reports on bioreactor-assisted baculovirus amplification is available, since most articles on large-scale production discuss the impact of the setup from the perspective of protein production (Caron et al. 1990; Mannix & Jarman 2000; Elias et al. 2007; Thompson et al. 2016; Weidner et al. 2017; Ghasemi et al. 2019). Simultaneously, no existing reports seem to discuss the effect of parameters typical for bioreactor setup on the behaviour and condition of the baculovirus itself. Nonetheless, it is worth to consider issues commonly highlighted in baculovirus-insect cell protein production studies, specifically, shear stress induced by stirring and aeration. While we, in our large-scale amplification, have taken measures to ensure gentle oxidation by using both micro- and macro-spargers, perhaps reviewing the stirring speed and aeration rate, as well as aeration method, could yield some clues for further investigation. As employed in some of the referenced papers on bioreactor studies, shifting to surface aeration (Caron et al. 1990) and lower DO concentration (Ghasemi et al. 2019) could be promising starting points to design a viable large-scale recombinant baculovirus amplification process.

Challenges with baculovirus production scale-up represent the second set of this thesis work's research goals that were partially fulfilled. Significant focus of the project was on developing this insect cell-based protein production and glycoengineering approach into a prerequisite for an industrial-grade platform, which would become a product of a novel biotechnology startup for tailoring *N*-linked oligosaccharides on commercial therapeutic IgGs. This objective requires established processes to be safe, robust, and scalable, and only some of the acquired results fit into the outlined criteria. We have ensured safety in all insect cell processes by maintaining exclusively chemically defined conditions. The main challenge with this aspect in the studied IVGE approach was found in the *N*-glycoprofile of produced and glycoengineered Rituximab from HighFive™, which contains noticeable presence of oligosaccharides with glycosidic linkages unnatural and immunogenic to humans (α1,3-linked fucose; α2,3-linked N-Acetylneuraminic acid). This especially concerns α1,3-linked core fucose, presumed on the dominant *N*-glycan species in our Rituximab product. To ensure clinical applicability of our IVGE setup, release of this particular core-linked sugar is necessary either through incorporation of a targeted fucosidase into the IVGE reaction cascade, or by switching the production cell line. Among Lepidopteran insect cells, Sf9 is reported to produce almost none α1,3-linked core fucose on glycoforms (Palomares et al. 2021), rendering it a possible alternative. However, switching antibody production to Sf9 would inevitably lead to significantly lower product yields than those expected from HighFive™, based on existing reports (Cérutti & Golay 2012; Palomares et al. 2021). Therefore, a careful consideration of a suitable approach to the safety enhancement of the IVGE strategy must be made.

Just like safety, robustness and scalability were not achieved to the full extent in this study. Promising results were obtained with glycosyltransferase production, as by the end of the thesis work, small-scale enzyme expression

protocol was established, extraction and purification setup was extensively optimized, narrowing down further troubleshooting options, and important limitations in scale-up of baculovirus platform were identified. So, despite lack of a complete scale-up strategy, important drafts for the enzyme production in insect cells have been made. As for the IVGE approach, glycan modification has only been tested using 45 µg of the starting antibody substrate, which is much less than the amounts routinely produced in industry, as those are in mg, g, and even kg scale (Kelley 2009). In addition, current database of the xCGE-LIF analysis software glyXtool^{MS} failed to identify *N*-glycan structures behind a number of peaks in the derived fingerprints, including the most prominent peaks. To strengthen the validity of the claimed IVGE success, and facilitate comprehensive assessment of insect cell glycans, an approach for definitive conformation of the unidentified *N*-glycan peak structures in the xCGE-LIF fingerprints needs to be introduced. This is particularly important to ensure safety of the product through reliable characterization of *N*-glycans with undesirable glycosidic linkages unnatural and immunogenic to humans (Mastrangeli et al. 2019), seen in HighFive™-produced Rituximab *N*-glycoprofile. Regarding antibody production in baculovirus-infected HighFive™, results were the furthest from the set objective. Extremely low amounts of therapeutic IgG_1 Rituximab were gathered, as expression was severely hindered by near complete lack of light and heavy chain assembly into the 150 kDa heterodimer. Lack of full-length antibody formation presents the most significant impediment for this novel IVGE approach, especially in the context of potential industrial application, and therefore needs to be thoroughly addressed to render the insect-cell based IVGE approach viable.

Thus, among the outlooks for further work on the project, the first recommended step would be tackling full-length antibody production. To establish the direction for optimization, critical evaluation of the completed work is needed to outline possible sources of poor IgG assembly. In a wide overview, our antibody production setup does not differ from the conditions employed by previous investigators who obtained fully-assembled IgGs, including Rituximab, through baculovirus infection of insect cells (Hasemann & Capra 1990; Nesbit et al. 1992; Edelman et al. 1997; Koch et al. 2003; Jar et al. 2009; Palmberger et al. 2011; Mabashi-Asazuma et al. 2014; Korn et al. 2020). Multiple scientific reports from various research groups that employed a range of Lepidopteran insect cells, primarily but not limited to Sf9 and HighFive™, demonstrate excellent chain assembly and formation of target IgGs. Majority of these studies used homologous recombination, for which recombinant baculoviruses were constructed using both commercial and in-house developed vectors and baculovirus generation systems. Interestingly, none of prior successful studies incorporated *flash*BAC™ ULTRA baculoviral DNA, like we did in this work. According to the manufacturer, *flash*BAC™ ULTRA and its compatible products have been extensively optimized for production of secreted proteins. Both baculoviral DNA and transfer vectors purchased from the manufacturer contain multiple features that ease the expression burden on infected cells: deletion of

non-essential late baculoviral genes that overload cellular machinery (*p10*, *p26*, *p74*, etc.); removal of most harmful viral proteins and proteases (chitinase, cathepsin); and incorporation of anti-apoptotic protein for extension of insect cell lifetime (vankyrin; for pOETV8.1 vectors only) (OET Ltd. 2019). Expectedly, by choosing this recombinant baculovirus generation platform, we ensured optimal conditions for infection progression in insect cells and target antibody quality. Also, the same platform performed well for our glycosyltransferase production, further solidifying its reliability. Together with choosing an advantageous baculovirus manufacturer, we incorporated key beneficial strategies for transfer vector design, found in the reference materials. Following clear preference for dual expression vectors in the literature, we used a dual vector construct for co-expression of two individual chains delivered in a single baculovirus; on top of that, we evaluated monopromoter vectors for co-infection with baculoviruses expressing individual chains, a less common strategy among the studied articles. Our construct assessment results were in line with the literature, as commercial dual transfer vector pOET5.1 from OET Ltd. managed to yield small fractions of an assembled antibody, thus outperforming monopromoter vectors pOET8.VE1, tested in co-infection in different ratios of light and heavy chain baculovirus. Furthermore, chain expression strategy for both dV and mV in this work was in agreement with existing research, which outlines the need for presence of light chain during heavy chain synthesis. As in most articles, for dV design, we utilized *p10* and *polh* promoters for light chain transcription (*p10* promoter) initiating several hours earlier than heavy chain transcription (*polh* promoter). For mV, we tested conditions with an excess of light chain baculovirus during co-infection of HighFive™ cells. Despite being reported as a crucial step in facilitating chain association into a full-length heterodimer (Cérutti & Golay 2012), this expression strategy failed to give us high-quality Rituximab. Other aspects of expression design of previous investigators align with our conditions as well. Specifically, referenced setup of experiments in suspension HighFive™ mostly matches those employed by us, especially in parameters like infection cell density (references: 1-4×10^6 cells/mL), MOI (0.1-20 IP/cell), and duration of infection (72-120 hpi). Even more, studied reports demonstrate equally effective IgG production using both chemically defined media (Jar et al. 2009; Korn et al. 2020), including ExpressFive™ (Koch et al. 2003) employed in our work, and media supplemented with additives like yeast extract and foetal bovine/calf serum (Hasemann & Capra 1990; Nesbit et al. 1992; Edelman et al., 1994; Palmberger et al. 2011). Notably, almost none of the reports utilize fed-batch strategy to produce IgGs in insect cells, since their non-supplemented batch processes yield desired product. In our work, despite sticking to the common recommendations in all aspects of expression setup, assembly of the target IgG was drastically low. Several steps of performed optimization, designed based on common recommendations for mammalian cell-based mAb production (Brühlmann et al. 2015), targeted improvement of infected HighFive™ cell condition and quality of Rituximab interchain disulphide bonds, and failed to facilitate complexation of individual chains. According to the Western blot

analysis, only minor improvements in antibody assembly were observed in fed-batch approach with daily supplementation, likely due to better cell condition induced by a steady supply of macro- and micronutrients. Tested additive Trehalose, investigated due to commonly attributed protein stabilizing properties (Olsson et al. 2016), resulted in target protein band differences too insignificant for further consideration. Meanwhile, supplementation of Cysteine as an oxidizing additive (Komuczki et al. 2022), as well as cell cultivation in the environment with enriched to 50% and carefully controlled dissolved oxygen levels, did not result in any evident effect on the target product. With that, we excluded recombinant baculovirus design, cell culture medium composition, and disulphide bond quality as sources of poor Rituximab assembly in our study.

Possible solutions to the antibody production dilemma might come from some of the oldest reports on efforts dedicated to IgG production in baculovirus-infected insect cells. According to several reviews, mAb fragmentation, detected in the earliest works, led to a hypothesis attributing poor antibody assembly to the inability of insect cell expression machinery to properly process proteins in the later stages of baculoviral infection, when endoplasmic reticulum (ER) is overloaded by active viral protein processing (Cérutti & Golay 2012). In addition, low levels of cytosolic and ER chaperone proteins in insect cells had been proposed to aggravate interchain association into a full heterodimer (Ailor & Betenbaugh 1998). To combat that, several approaches were assessed in subsequent studies, namely, co-expression of molecular chaperone proteins with the target antibody (Hsu et al. 1994), replacement of late baculoviral promoters (*p10*, *polh*) in transfer vector constructs with early (*ie1/2*), and switching from transiently infected antibody-expressing cell cultures to stable cell lines (Cérutti & Golay 2012). All of these recommendations demonstrated significant improvement of formation of full-length antibodies. Unfortunately, these approaches do not explain why the fragmentation was displayed by HighFive™ cell line in our study, while other investigators have successfully produced well assembled mAbs under similar conditions throughout the last thirty years. Yet, since the construct design strategies had been confirmed effective, proposed directions for further work on this project focus on them. For the main purpose of the IVGE strategy, remodelling dual transfer vector constructs to contain early baculoviral promoters instead of current very late *p10* and *polh*, or chaperone sequences in presence of *p10* and *polh* promoters, would be recommended. Chaperone protein family Hsp70 is especially suggested due to confirmed enhancement of secreted assembled IgG levels (Yokoyama et al. 2000). Alternatively, baculovirus-free expression approaches are proposed to avoid the complications associated with the viral burden on the insect cells. Korn et al. (2020) demonstrated excellent performance in IgG expression of HighFive™ cells, transiently transfected using polyethylenimine, giving a solid option for consideration if transient expression remains in priority for the current project. Otherwise, stable cell line development approach might be worth investigating to develop setup suitable for long-term production of mAbs of choice, thus

matching commonly employed stable cell line generation practice in industrial mAb manufacturing (Zhu et al. 2017).

Altogether, a number of issues require attention in the immediate future of this IVGE project. Significant effort is needed to finalize enzyme purification strategy, where more extensive assessment of the solubilizing additive in buffer formulation is to be done, as well as incorporation of an additional purification step for purity improvement, such as size exclusion chromatography. Substantial optimization of antibody expression strategy is another even more important step, where re-design of expression construct and potential remodelling of the expression platform itself seems to be necessary. Finally, for the IVGE strategy, a more in-depth assessment of performance of glycosyltransferases produced in insect cells would be required; upon selecting suitable working conditions of the enzymes, starting amounts of, hopefully, high-quality antibody material should undergo scale-up to satisfy industrial-scale ambitions of this project. With the functional production setup, glycoengineered antibody can be put through functionality testing to assess its biological and effector properties proving its functionality and suitability for clinical use. Meanwhile, an expansion of the glyXtool^{MS} database for insect cell glycoforms would facilitate reliable annotation of oligosaccharides analysed with xCGE-LIF method. Alternatively, the platform requires implementation of an orthogonal method for *N*-glycan identification, such as matrix-assisted laser desorption/ionization time-of-flight mass spectrometry (MALDI-TOF-MS), routinely utilized for this purpose (Illiano et al. 2020). Hopefully, key outcomes of the current investigation, paired with the outlined directions for optimization, shall boost the chances of achieving a high-performing setup. Yet, even with all faults fixed, this *in vitro* glycoengineering strategy would be far from complete. As discussed earlier, ''ideal'' *N*-linked oligosaccharides for therapeutic mAbs lack core fucoses, and contain two fully galactosylated antennas with terminal sialic acids. Even at the finest state of the evaluated IVGE procedure, only complete galactosylation is achieved. Without attaching terminal α2,6-linked N-Acetylneuraminic acid and removing core α1,3/6-linked fucose, attractiveness of this platform is easily lost, as core fucosylation is the strongest inhibitor for ADCC (Mastrangeli et al. 2019), and terminal sialic acids are necessary for extended half-life of mAbs in patients' blood sera (Dammen-Brower et al. 2022). To gain these benefits, the project needs a fucosidase candidate capable of catalysing hydrolysis of both α1,3 and α1,6 glycosidic linkages (for HighFive™-based production), or α1,6 glycosidic linkage (for Sf9-based production), and a sialyltransferase able to add both N-Acetylneuraminic acid moieties by catalysing establishment of the correct α2,6 linkage (Figure 14). Therefore, work towards the platform offering product that maximizes therapeutic mAb potential is set to continue in the near future. Nonetheless, with the prerequisite work done in this Master thesis project, created proof-of-concept for the novel IgG *in vitro* chemoenzymatic modification, and thoroughly established directions for improvement, a powerful IVGE toolbox may emerge soon in the academic and industrial environment dedicated to therapeutic proteins, mAbs included.

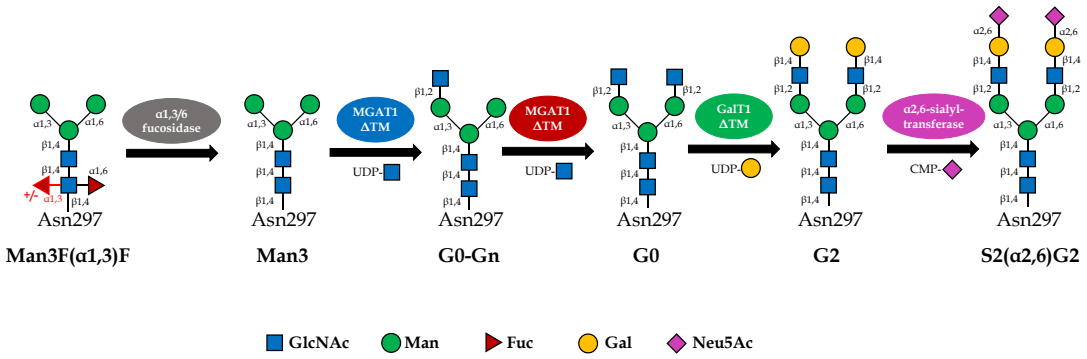

Figure 14. Product vision for insect cell-based IVGE strategy designed for therapeutic mAb modulation. Dominant *N*-glycan Man3(α1,3)F, produced by HighFive™ insect cells on an antibody, is afucosylated by an α1,3/6-fucosidase, resulting in Man3. Man3 core is then elongated by sequential attachment of GlcNAc and Gal residues, as performed in the current IVGE approach. To the resulting terminally galactosylated G2 structure, Neu5Ac moieties are attached by an α2,6 -sialyltransferase. Illustrated structures represent *N*-glycans attached to position Asn297 of an intact IgG antibody. Activated monosaccharides are carried by a signalling molecule Uridine Diphosphate (UDP) or cytidine-5'-monophosphate (CMP). GlcNAc corresponds to N-Acetylglucosamine, Man to Mannose, Fuc to Fucose, Gal to Galactose, Neu5Ac to N-Acetylneuraminic acid.

REFERENCES

Ailor, E., & Betenbaugh, M. J. (1998). Overexpression of a cytosolic chaperone to improve solubility and secretion of a recombinant IgG protein in insect cells. *Biotechnology and Bioengineering*, 58(2–3), 196–203.

Alberts, B., Johnson, A., Lewis, J., Raff, M., Roberts, K., & Walter, P. (2002). B Cells and Antibodies. In *Molecular Biology of the Cell*. 4th edition. Garland Science. https://www.ncbi.nlm.nih.gov/books/NBK26884/

Brühlmann, D., Jordan, M., Hemberger, J., Sauer, M., Stettler, M., & Broly, H. (2015). Tailoring recombinant protein quality by rational media design. Biotechnology Progress, 31(3), 615–629. https://doi.org/10.1002/btpr.2089

Caron, A. W., Archambault, J., & Massie, B. (1990). High-level recombinant protein production in bioreactors using the baculovirus-insect cell expression system. *Biotechnology and Bioengineering*, 36(11), 1133–1140. https://doi.org/10.1002/bit.260361108

Cérutti, M., & Golay, J. (2012). Lepidopteran cells, an alternative for the production of recombinant antibodies? *mAbs*, 4(3), 294–309. https://doi.org/10.4161/mabs.19942

Chung, S.-W., Joo, H.-S., Jang, K.-S., Lee, H.-J., Lee, S.-G., & Kim, B.-G. (2006). Galactosylation and sialylation of terminal glycan residues of human immunoglobulin G using bacterial glycosyltransferases with in situ regeneration of sugar-nucleotides. *Enzyme and Microbial Technology*, 39(1), 60–66. https://doi.org/10.1016/j.enzmictec.2005.09.007

Dammen-Brower, K., Epler, P., Zhu, S., Bernstein, Z. J., Stabach, P. R., Braddock, D. T., Spangler, J. B., & Yarema, K. J. (2022). Strategies for Glycoengineering Therapeutic Proteins. *Frontiers in Chemistry*, 10, 863118. https://doi.org/10.3389/fchem.2022.863118

Ds, D. (2012). Therapeutic proteins. Methods in Molecular Biology (Clifton, N.J.), 899. https://doi.org/10.1007/978-1-61779-921-1_1

Dumont, J., Euwart, D., Mei, B., Estes, S., & Kshirsagar, R. (2016). Human cell lines for biopharmaceutical manufacturing: History, status, and future perspectives. *Critical Reviews in Biotechnology*, 36(6), 1110–1122. https://doi.org/10.3109/07388551.2015.1084266

Edelman, L., Margaritte, C., Chaabihi, H., Monchâtre, E., Blanchard, D., Cardona, A., Morin, F., Dumas, G., Petres, S., & Kaczorek, M. (1997). Obtaining a functional recombinant anti-rhesus (D) antibody using the baculovirus-insect cell expression system. *Immunology*, 91(1), 13–19.

Elias, C. B., Jardin, B., & Kamen, A. (2007). Recombinant protein production in large-scale agitated bioreactors using the baculovirus expression vector system. *Methods in Molecular Biology* (Clifton, N.J.), 388, 225–246. https://doi.org/10.1007/978-1-59745-457-5_11

Gagneux, P., Hennet, T., & Varki, A. (2022). Biological Functions of Glycans. In A. Varki, R. D. Cummings, J. D. Esko, P. Stanley, G. W. Hart, M. Aebi, D. Mohnen, T. Kinoshita, N. H. Packer, J. H. Prestegard, R. L. Schnaar, & P. H.

Seeberger (Eds.), Essentials of Glycobiology (4th ed.). Cold Spring Harbor Laboratory Press. http://www.ncbi.nlm.nih.gov/books/NBK579984/

Ghasemi, A., Bozorg, A., Rahmati, F., Mirhassani, R., & Hosseininasab, S. (2019). Comprehensive study on Wave bioreactor system to scale up the cultivation of and recombinant protein expression in baculovirus-infected insect cells. *Biochemical Engineering Journal*, 143, 121–130. https://doi.org/10.1016/j.bej.2018.12.011

Hasemann, C. A., & Capra, J. D. (1990). High-level production of a functional immunoglobulin heterodimer in a baculovirus expression system. *Proceedings of the National Academy of Sciences of the United States of America*, 87(10), 3942–3946. https://doi.org/10.1073/pnas.87.10.3942

Higel, F., Seidl, A., Sörgel, F., & Friess, W. (2016). N-glycosylation heterogeneity and the influence on structure, function and pharmacokinetics of monoclonal antibodies and Fc fusion proteins. *European Journal of Pharmaceutics and Biopharmaceutics*, 100, 94–100. https://doi.org/10.1016/j.ejpb.2016.01.005

Hsu, T. A., Eiden, J. J., Bourgarel, P., Meo, T., & Betenbaugh, M. J. (1994). Effects of co-expressing chaperone BiP on functional antibody production in the baculovirus system. *Protein Expression and Purification*, 5(6), 595–603. https://doi.org/10.1006/prep.1994.1082

Illiano, A., Pinto, G., Melchiorre, C., Carpentieri, A., Faraco, V., & Amoresano, A. (2020). Protein Glycosylation Investigated by Mass Spectrometry: An Overview. *Cells*, 9(9), 1986. https://doi.org/10.3390/cells9091986

Ja, M., Ot, R., & La, P. (2003). Titration of non-occluded baculovirus using a cell viability assay. *BioTechniques*, 34(2). https://doi.org/10.2144/03342bm05

Jar, A. M., Osorio, F. A., & López, O. J. (2009). Mouse × pig chimeric antibodies expressed in Baculovirus retain the same properties of their parent antibodies. *Biotechnology Progress*, 25(2), 516–523. https://doi.org/10.1002/btpr.113

Jaroentomeechai, T., Kwon, Y. H., Liu, Y., Young, O., Bhawal, R., Wilson, J. D., Li, M., Chapla, D. G., Moremen, K. W., Jewett, M. C., Mizrachi, D., & DeLisa, M. P. (2022). A universal glycoenzyme biosynthesis pipeline that enables efficient cell-free remodeling of glycans. *Nature Communications*, 13(1), 6325. https://doi.org/10.1038/s41467-022-34029-7

Kelley, B. (2009). Industrialization of mAb production technology: The bioprocessing industry at a crossroads. *mAbs*, 1(5), 443–452. https://doi.org/10.4161/mabs.1.5.9448

Koch, J., Liang, M., Queitsch, I., Kraus, A. A., & Bautz, E. K. F. (2003). Human recombinant neutralizing antibodies against hantaan virus G2 protein. *Virology*, 308(1), 64–73. https://doi.org/10.1016/S0042-6822(02)00094-6

Komuczki, D., Stadermann, A., Bentele, M., Unsoeld, A., Grillari, J., Mueller, M., Paul, A., & Fischer, S. (2022). High cysteine concentrations in cell culture media lead to oxidative stress and reduced bioprocess performance of recombinant CHO cells. *Biotechnology Journal*, 17. https://doi.org/10.1002/biot.202200029

Korn, J., Schäckermann, D., Kirmann, T., Bertoglio, F., Steinke, S., Heisig, J., Ruschig, M., Rojas, G., Langreder, N., Wenzel, E. V., Roth, K. D. R., Becker, M., Meier, D., van den Heuvel, J., Hust, M., Dübel, S., & Schubert, M. (2020). Baculovirus-free insect cell expression system for high yield antibody and antigen production. *Scientific Reports*, 10(1), 21393. https://doi.org/10.1038/s41598-020-78425-9

Leibly, D. J., Nguyen, T. N., Kao, L. T., Hewitt, S. N., Barrett, L. K., & Van Voorhis, W. C. (2012). Stabilizing Additives Added during Cell Lysis Aid in the Solubilization of Recombinant Proteins. *PLoS ONE*, 7(12), e52482. https://doi.org/10.1371/journal.pone.0052482

Lu, L. L., Suscovich, T. J., Fortune, S. M., & Alter, G. (2018). Beyond binding: Antibody effector functions in infectious diseases. *Nature Reviews Immunology*, 18(1), 46–61. https://doi.org/10.1038/nri.2017.106

Ma, B., Guan, X., Li, Y., Shang, S., Li, J., & Tan, Z. (2020). Protein Glycoengineering: An Approach for Improving Protein Properties. *Frontiers in Chemistry*, 8. https://doi.org/10.3389/fchem.2020.00622

Mabashi-Asazuma, H., Kuo, C.-W., Khoo, K.-H., & Jarvis, D. L. (2014). A novel baculovirus vector for the production of nonfucosylated recombinant glycoproteins in insect cells. *Glycobiology*, 24(3), 325–340. https://doi.org/10.1093/glycob/cwt161

Mannix, C., & Jarman, R. F. (2000). *A Guide to Successful Scale-up of the Baculovirus Expression System* (M. Al-Rubeai, Ed.; Vol. 2, pp. 43–55). Springer Netherlands. https://doi.org/10.1007/978-94-011-4315-8_3

Marichal-Gallardo, P., Börner, K., Pieler, M. M., Sonntag-Buck, V., Obr, M., Bejarano, D., Wolff, M. W., Kräusslich, H.-G., Reichl, U., & Grimm, D. (2021). Single-Use Capture Purification of Adeno-Associated Viral Gene Transfer Vectors by Membrane-Based Steric Exclusion Chromatography. *Human Gene Therapy*, 32(17–18), 959–974. https://doi.org/10.1089/hum.2019.284

Mimura, Y., Katoh, T., Saldova, R., O'Flaherty, R., Izumi, T., Mimura-Kimura, Y., Utsunomiya, T., Mizukami, Y., Yamamoto, K., Matsumoto, T., & Rudd, P. M. (2018). Glycosylation engineering of therapeutic IgG antibodies: Challenges for the safety, functionality and efficacy. *Protein & Cell*, 9(1), 47–62. https://doi.org/10.1007/s13238-017-0433-3

Moremen, K. W., Ramiah, A., Stuart, M., Steel, J., Meng, L., Forouhar, F., Moniz, H. A., Gahlay, G., Gao, Z., Chapla, D., Wang, S., Yang, J.-Y., Prabhakar, P. K., Johnson, R., Rosa, M. D., Geisler, C., Nairn, A. V., Seetharaman, J., Wu, S.-C., … Jarvis, D. L. (2018). Expression system for structural and functional studies of human glycosylation enzymes. *Nature Chemical Biology*, 14(2), 156–162. https://doi.org/10.1038/nchembio.2539

Mota, L. M., Tayi, V. S., & Butler, M. (2022). Cell Free Remodeling of Glycosylation of Antibodies. *Methods in Molecular Biology* (Clifton, N.J.), 2370, 117–146. https://doi.org/10.1007/978-1-0716-1685-7_6

Neelamegham, S., Aoki-Kinoshita, K., Bolton, E., Frank, M., Lisacek, F., Lütteke, T., O'Boyle, N., Packer, N. H., Stanley, P., Toukach, P., Varki, A., Woods, R. J., & SNFG Discussion Group. (2019). Updates to the Symbol Nomenclature

for Glycans guidelines. *Glycobiology*, 29(9), 620–624. https://doi.org/10.1093/glycob/cwz045

Nesbit, M., Fu, Z. F., McDonald-Smith, J., Steplewski, Z., & Curtis, P. J. (1992). Production of a functional monoclonal antibody recognizing human colorectal carcinoma cells from a baculovirus expression system. *Journal of Immunological Methods*, 151(1–2), 201–208. https://doi.org/10.1016/0022-1759(92)90118-d

Oxford Expression Technologies. 2016. Baculovirus Gene Mutations and Protein Expression. News&Blog post. Accessed 23.02.2024. https://www.oetltd.com/post/baculovirus-gene-mutations-and-protein-expression

Oxford Expression Technologies. 2019. *baculo*COMPLETE User Guide: A Complete Laboratory Guide to theBaculovirus Expression System and Insect Cell Culture. Accessed 05.01.2024.

Olsson, C., Jansson, H., & Swenson, J. (2016). The Role of Trehalose for the Stabilization of Proteins. *The Journal of Physical Chemistry*. B, 120(20), 4723–4731. https://doi.org/10.1021/acs.jpcb.6b02517

Palmberger, D., Rendić, D., Tauber, P., Krammer, F., Wilson, I. B. H., & Grabherr, R. (2011). Insect cells for antibody production: Evaluation of an efficient alternative. *Journal of Biotechnology*, 153(3), 160–166. https://doi.org/10.1016/j.jbiotec.2011.02.009

Palomares, L. A., Srivastava, I. K., Ramírez, O. T., & Cox, M. M. J. (2021). Glycobiotechnology of the Insect Cell-Baculovirus Expression System Technology. *Advances in Biochemical Engineering/Biotechnology*, 175, 71–92. https://doi.org/10.1007/10_2018_61

Raju, T. S., Briggs, J. B., Chamow, S. M., Winkler, M. E., & Jones, A. J. S. (2001). Glycoengineering of Therapeutic Glycoproteins: In Vitro Galactosylation and Sialylation of Glycoproteins with Terminal N-Acetylglucosamine and Galactose Residues. *Biochemistry*, 40(30), 8868–8876. https://doi.org/10.1021/bi010475i

Ruhnau, J., Grote, V., Juarez-Osorio, M., Bruder, D., Mahour, R., Rapp, E., Rexer, T. F. T., & Reichl, U. (2021). Cell-Free Glycoengineering of the Recombinant SARS-CoV-2 Spike Glycoprotein. *Frontiers in Bioengineering and Biotechnology*, 9, 699025. https://doi.org/10.3389/fbioe.2021.699025

Stanley, P., Schachter, H., & Taniguchi, N. (2009). N-Glycans. In A. Varki, R. D. Cummings, J. D. Esko, H. H. Freeze, P. Stanley, C. R. Bertozzi, G. W. Hart, & M. E. Etzler (Eds.), *Essentials of Glycobiology* (2nd ed.). Cold Spring Harbor Laboratory Press. http://www.ncbi.nlm.nih.gov/books/NBK1917/

Thompson, C. M., Montes, J., Aucoin, M. G., & Kamen, A. A. (2016). Recombinant Protein Production in Large-Scale Agitated Bioreactors Using the Baculovirus Expression Vector System. *Methods in Molecular Biology* (Clifton, N.J.), 1350, 241–261. https://doi.org/10.1007/978-1-4939-3043-2_11

Varki, A., Cummings, R. D., Esko, J. D., Stanley, P., Hart, G. W., Aebi, M., Darvill, A. G., Kinoshita, T., Packer, N. H., Prestegard, J. H., Schnaar, R. L., & Seeberger, P. H. (Eds.). (2015). *Essentials of Glycobiology* (3rd ed.). Cold

Spring Harbor Laboratory Press. http://www.ncbi.nlm.nih.gov/books/NBK310274/

Weidner, T., Druzinec, D., Mühlmann, M., Buchholz, R., & Czermak, P. (2017). The components of shear stress affecting insect cells used with the baculovirus expression vector system. *Zeitschrift Für Naturforschung C*, 72(9–10), 429–439. https://doi.org/10.1515/znc-2017-0066

Wiśniewski, J. R., Zougman, A., Nagaraj, N., & Mann, M. (2009). Universal sample preparation method for proteome analysis. *Nature Methods*, 6(5), 359–362. https://doi.org/10.1038/nmeth.1322

Xu, W.-J., Lin, Y., Mi, C.-L., Pang, J.-Y., & Wang, T.-Y. (2023). Progress in fed-batch culture for recombinant protein production in CHO cells. *Applied Microbiology and Biotechnology*, 107(4), 1063–1075. https://doi.org/10.1007/s00253-022-12342-x

Yokoyama, N., Hirata, M., Ohtsuka, K., Nishiyama, Y., Fujii, K., Fujita, M., Kuzushima, K., Kiyono, T., & Tsurumi, T. (2000). Co-expression of human chaperone Hsp70 and Hsdj or Hsp40 co-factor increases solubility of overexpressed target proteins in insect cells. *Biochimica et Biophysica Acta (BBA) - Gene Structure and Expression*, 1493(1), 119–124. https://doi.org/10.1016/S0167-4781(00)00170-6

Zhang, J.-H., Shan, L.-L., Liang, F., Du, C.-Y., & Li, J.-J. (2022). Strategies and Considerations for Improving Recombinant Antibody Production and Quality in Chinese Hamster Ovary Cells. *Frontiers in Bioengineering and Biotechnology*, 10, 856049. https://doi.org/10.3389/fbioe.2022.856049

Zhu, M. M., Mollet, M., Hubert, R. S., Kyung, Y. S., & Zhang, G. G. (2017). Industrial Production of Therapeutic Proteins: Cell Lines, Cell Culture, and Purification. *Handbook of Industrial Chemistry and Biotechnology*, 1639–1669. https://doi.org/10.1007/978-3-319-52287-6_29

APPENDIX 1. MAPS OF TRANSFER VECTOR CONSTRUCTS FOR ANTIBODY EXPRESSION

TABLE 6. Clarifications of components of transfer vectors encoding Rituximab used in this study.

Label	Clarification
M13 fwd	M13 Forward Primer
M13 rev	M13 Reverse Primer
bla promoter	Promoter for expression of the ampicillin resistance gene in *E.coli*
ori	Origin of replication

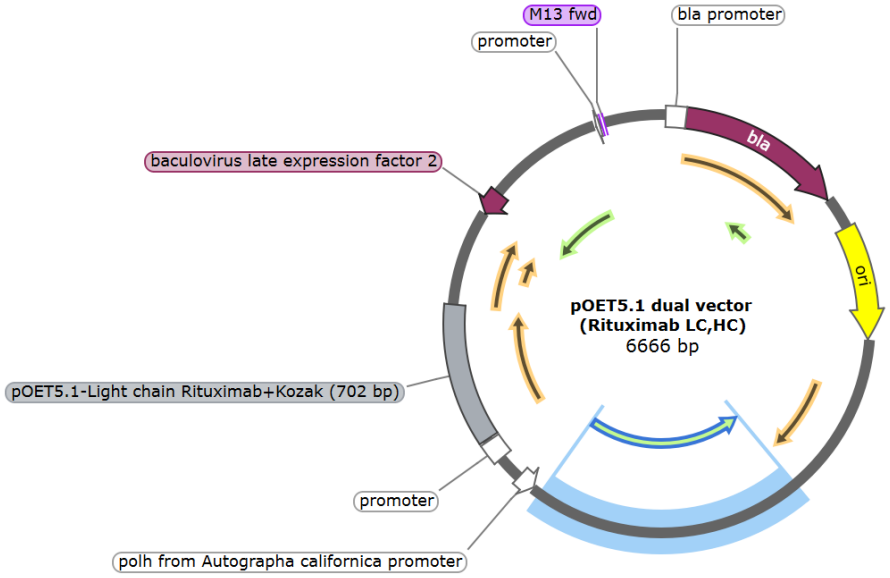

Figure 15. Map of dual promoter vector pOET5.1 (OET Ltd.) with inserted sequences of Rituximab light and heavy chains, and supporting components. Map region highlighted in blue represents Rituximab heavy chain sequence with Kozak sequence (1395 bp). Vector map produced in SnapGene Viewer.

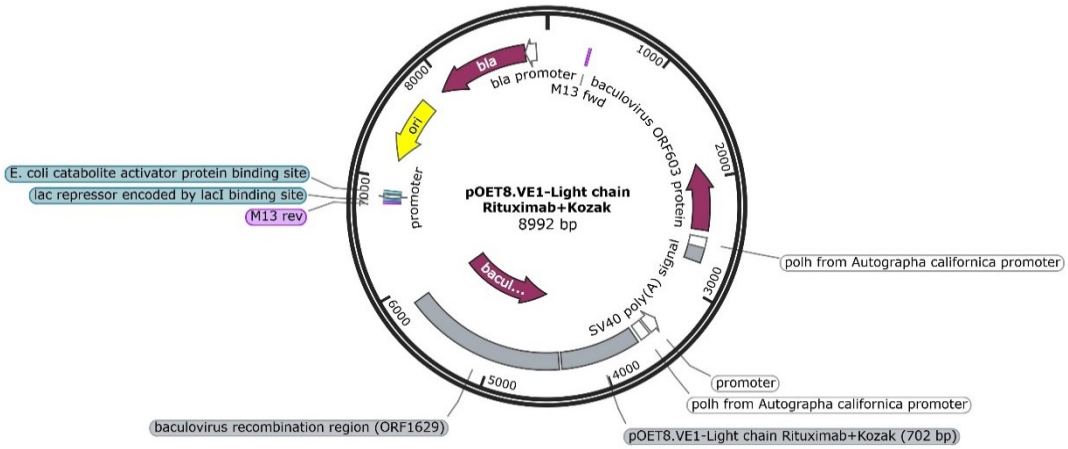

Figure 16. Map of monopromoter transfer vector pOET8.VE1 (OET Ltd.) with inserted sequence of Rituximab light chain, and supporting components. Vector map produced in SnapGene Viewer.

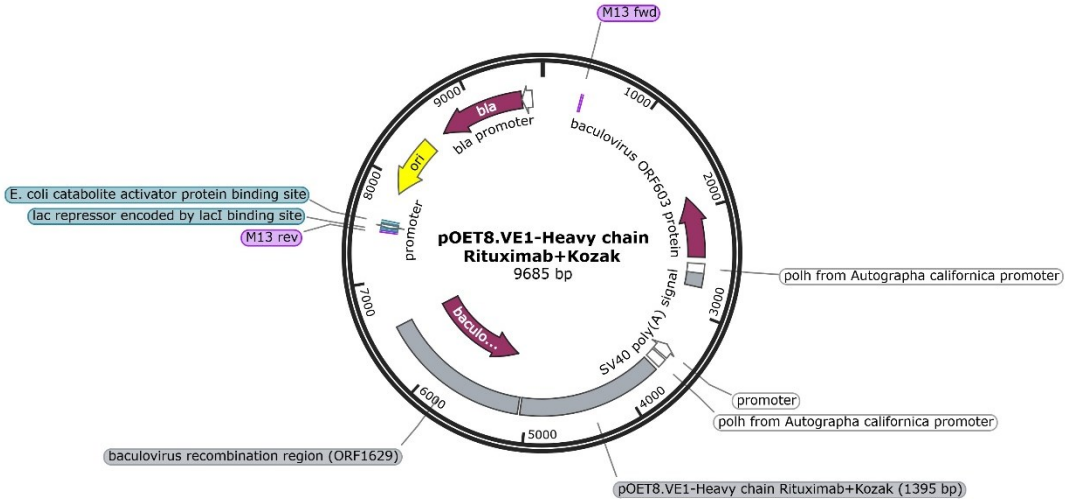

Figure 17. Map of monopromoter transfer vector pOET8.VE1 (OET Ltd.) with inserted sequence of Rituximab heavy chain, and supporting components. Vector map produced in SnapGene Viewer.